Preprint typeset in JINST style - HYPER VERSION

ATLAS Pixel Detector Mechanics and Services

G. Aad[10], M. Ackers[2], F.A. Alberti[11], M. Aleppo[11], G. Alimonti[11], J. Alonso[1], E.C. Anderssen[1], A. Andreani[11], A. Andreazza[11], J-F. Arguin[1], K.E. Arms[13], D. Barberis[7], M.B. Barbero[2], M. Bazalova[15], R.B. Beccherle[7], K.H. Becks[20], P.K. Behera[8], F. Bellina[20], J. Beringer[1], K. Bernardet[10], J.B. Biesiada[1], L. Blanquart[1], J. Boek[20], G.R. Boyd[14], P. Breugnon[10], P. Buchholz[17], B. Butler[16], M. Caccia[11], A.C. Capsoni[11], C. Caso[7,*], D. Cauz[19], M. Cepeda[1], R. Cereseto[7], M. Cervetto[7], M.L. Chu[18], M. Citterio[11], J.C. Clemens[10], Y.C. Coadou[3], M. Cobal[19], A. Coccaro[7], S. Coelli[11], S. Correard[10], M. Cristinziani[2], S. Cuneo[7], S. D'Auria[19], M. Dameri[7], G. Darbo[7], S. Dardin[1], B. De Lotto[19], U. De Sanctis[11], J.B. De Vivie De Regie[10], C. Del Papa[19], P. Delpierre[10], B. Di Girolamo[3], W. Dietsche[2], F. Djama[10], D. Dobos[6], M. Donega[3], J. Dopke[20], K. Einsweiler[1], A. Eyring[2], L. Feligioni[10], W. Fernando[13], P. Fischer[2], M.J. Fisher[13], T. Flick[20], G. Gagliardi[7], E. Galyaev[5], K.K. Gan[13], M. Garcia-Sciveres[1], N. Garelli[7], G.G. Gariano[7], G.G. Gaycken[2], C. Gemme[7], P. Gerlach[20], M. Gilchriese[1], M.P. Giordani[19], D. Giugni[11], K.W. Glitza[20], C. Gössling[6], T. Golling[1], F. Goozen[1], I. Gorelov[12], G. Gorfine[20], C. Grah[20], H.M. Gray[4], I.M. Gregor[20], J. Grosse-Knetter[2], K. Grybel[17], P. Gutierrez[14], G.D. Hallewell[10], N. Hartman[1], M. Havranek[15], B. Heinemann[1], T. Henß[20], M.R. Hoeferkamp[12], D. Hoffmann[10], M. Holder[17], W. Honerbach[2], C. Horn[16], S. Hou[18], G.S. Huang[14], F. Huegging[2], E. Hughes[4], I. Ibragimov[17], I. Ilyashenko[3], M. Imhaeuser[20], J.M. Izen[5], J. Jackson[13], D. Jana[14], R.C. Jared[1], P. Jez[15], T. Johnson[1], J. Joseph[1], H. Kagan[13], M. Karagounis[2], R.D. Kass[13], M. Keil[2], S. Kersten[20], P. Kind[20], J. Klaiber-Lodewigs[6], L. Klingbeil[2], R. Klingenberg[6], A. Korn[1], V.V. Kostyukhin[7], I. Kostyukhina[7], O. Krasel[6], H. Krüger[2], K. Krueger[1], J. Kudlaty[6], T. Kuhl[2], O. Kvasnicka[15], K. Lantzsch[20], T. Lari[11], S.L. Latorre[11], S.C. Lee[18], T. Lenz[20], G. Lenzen[20], J. Lepidis[20], J. Levêque[10], M. Leyton[1], D. Lopez Mateos[4], K. F. Loureiro[13], D. Lüke[6], L. Luisa[19], J. Lys[1], R. J. Madaras[1], P. Mättig[20], F.M. Manca[11], E. Mandelli[1], M. Marcisovsky[15], Z. Marshall[4], G. Martinez[2], L.M. Masetti[2], M. Maß[6], M. Mathes[2], R. McKay[9], G. Meddeler[1], R. Meera-Lebbai[14], C. Meroni[11], J. Metcalfe[12], W.T. Meyer[9], D.W. Miller[16], W. Miller[1], S. Montesano[11], M.M. Monti[11], P. Morettini[7], J.M. Moss[13], T. Mouthuy[10], P. Nechaeva[7], W. Ockenfels[2], G.A. Odino[7], M. Olcese[7], B. Osculati[7], F. Parodi[7], A. Pekedis[1], K. Perez[4], I. Peric[2], C. Pizzorno[7], J. Popule[15], R. Post[1], F. Ragusa[11], A.M. Rahimi[13], B. Raith[2], S. Rajek[6], K. Reeves[20], I. Reisinger[6], J.D. Richardson[1], E. I. Rosenberg[9], L. P. Rossi[7], I. Rottländer[2], A.R. Rovani[7], A. Rozanov[10], O. Runolfsson[2], E.R. Ruscino[7], A.F. Saavedra[1], F.S. Sabatini[11], M. Saleem[14], S. Sandvoss[20], B. Sanny[20], L. Santi[19], M.I. Scherzer[1], C. Schiavi[7], A. Schreiner[8], J. Schultes[20], A. Schwartzman[16], R. Seibert[17], S.C. Seidel[12], H. Severini[14], S. Shanava[3], P. Sicho[15], P. Skubic[14], A.C. Smith[1], D.S. Smith[13], J. Snow[14], T. Stahl[17], T. Stockmanns[2], S. Strandberg[1], M. Strauss[14], D. Ta[2], F. Tegenfeldt[9], P.K. Teng[18], R. Ter-Antonyan[13], J. Thadome[20], T. Tic[15], L. Tomasek[15], M. Tomasek[15], F. Tomasi[11], K. Toms[12], C. Tran[1], J. Treis[2], N. Triplett[9], C. Troncon[11], L. Vacavant[10], S. Vahsen[1], J. Valenta[15], G. Vegni[11], F. Vernocchi[7], E. Vigeolas[10], J. Virzi[1], E. Viscione[11], V. Vrba[15], J. Walbersloh[6], W. Walkowiak[17], J. Weber[6], T.F. Weber[1], J. Weingarten[6], C. Weldon[1], N. Wermes[2], U. Werthenbach[17], J.S. Wirth[1], R. Witharm[1], B. Witt[20], M. Wittgen[16], J. Wuestenfeld[6], R. Wunstorf[6], J. Wyckoff[1], W-M. Yao[1], C. Young[16], R. Zaidan[10], M. Zdrazil[1], F. Zetti[1], J. Zhong[18], M. Ziolkowski[17], G. Zizka[1] and M.M. Zoeller[13]

[1]*Lawrence Berkeley National Laboratory and University of California, Physics Division*
MS50B-6227, 1 Cyclotron Road, Berkeley, CA 94720, United States of America
[2]*Physikalisches Institut der Universität Bonn*
Nussallee 12, D - 53115 Bonn, Germany
[3]*CERN*
CH - 1211 Geneva 23, Switzerland
[4]*Columbia University, Nevis Laboratory*
136 So. Broadway, Irvington, NY 10533, United States of America
[5]*University of Texas at Dallas*
800 West Campbell Road, Richardson, TX 75080-3021, United States of America
[6]*Universität Dortmund, Experimentelle Physik IV*
DE - 44221 Dortmund, Germany
[7]*INFN Genova and Università di Genova, Dipartimento di Fisica*
via Dodecaneso 33, IT - 16146 Genova, Italy
[8]*University of Iowa*
203 Van Allen Hall, Iowa City IA 52242-1479, United States of America
[9]*Iowa State University, Dept of Physics and Astronomy,Ames High Energy Physics Group*
Ames, IA 50011-3160, United States of America
[10]*CPPM, Aix-Marseille Université*
CNRS/IN2P3, Marseille, France
[11]*INFN Milano and Università di Milano, Dipartimento di Fisica*
via Celoria 16, IT - 20133 Milano, Italy
[12]*Department of Physics and Astronomy, University of New Mexico*
Albuquerque, NM 87131, United States of America
[13]*Ohio State University*
191 West Woodruff Ave, Columbus, OH 43210-1117, United States of America
[14]*University of Oklahoma, Homer L. Dodge Department of Physics*
440 West Brooks, Room 100, Norman, OK 73019-0225, United States of America
[15]*Institute of Physics, Academy of Sciences of the Czech Republic*
Na Slovance 2, CZ - 18221 Praha 8, Czech Republic
[16]*Stanford Linear Accelerator Center*
Stanford, California 94309, United States of America
[17]*Universität Siegen, Fachbereich Physik*
DE - 57068 Siegen, Germany
[18]*Insitute of Physics, Academia Sinica*
TW - Taipei 11529, Taiwan
[19]*INFN Gruppo Collegato di Udine and Università di Udine, Dipartimento di Fisica*
via delle Scienze 208, IT - 33100 Udine, Italy
[20]*Bergische Universität, Fachbereich C, Physik*
Postfach 100127, Gauss-Strasse 20, DE- 42097 Wuppertal, Germany
[*]*Deceased*
Corressponding author: M. Gilchriese: MGGilchriese@lbl.gov

ABSTRACT: The silicon pixel tracking system for the ATLAS experiment at the Large Hadron Collider is described and the performance requirements are summarized. Detailed descriptions of the pixel detector electronics and the silicon sensors are given. The design, fabrication, assembly and performance of the pixel detector modules is presented. Data obtained from test beams as well as studies using cosmic rays are also discussed.

KEYWORDS: Particle tracking detectors;ATLAS;LHC.

Contents

1. Introduction

2. Overview

The mechanical elements and services of the pixel detector are described in this section. We also describe the integration of the major components of the pixel detector and installation in ATLAS. The pixel detector, including the internal services, is located within the pixel support tube (PST) as already shown in Figure 2.1. A perspective view of the pixel detector elements within the PST is shown in Figure 1.

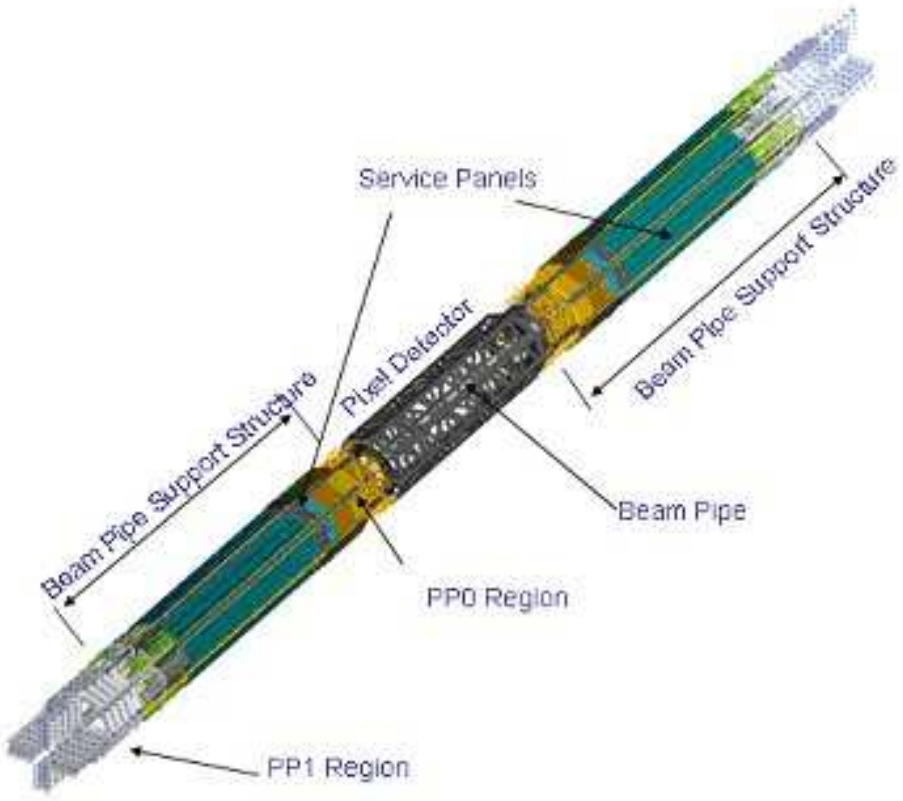

Figure 1. A perspective view of the active region of the pixel detector and of the internal pixel services and related support structures.

The active regions of the pixel detector are divided into a barrel region and two identical endcaps. The active elements in the barrel region are staves (with integrated cooling) each supporting 13 modules. The staves are held precisely by half-shells that are joined to form the three barrel layers of the detector. The active elements in the endcap regions are disk sectors (also with integrated cooling) each supporting six modules. Eight disk sectors are supported on a disk support ring. There are three disks in each of the two endcaps. The design and construction of these barrel and endcap elements are described in subsequent sections of this chapter.

The barrel shells and the disk rings are rigidly supported by a support frame constructed in three sections âĂŞ a barrel section and two identical endcap sections. The support frame is constructed from carbon composites apart from small aluminum blocks in the regions where the barrel and endcap frame sections are bolted together. A picture of the support frame is shown in Figure 2. Four precision mounts are mounted on endplates attached to the support frame. These precision mounts engage mating supports in the PST when the support frame and the attached services slide through the PST during the installation procedure(section 7.7).

Figure 2. The support frame for the pixel detector.

The beryllium beam pipe [Ref] within the ATLAS detector is held on each side of the support frame by additional composite structures, the Beam Pipe Support Structure (BPSS). The BPSS also supports the Service Quarter Panels (SQP) that contain coolant pipes and all electrical services for the pixel modules [Section 6]. A low mass cable from each pixel module (Type 0 cable) is connected to the SQPs via small connectors at Patch Panel 0 (PP0 âĂŞ see Figure 1). The connections to the external services for the pixel detector are made to the SQPs at Patch Panel 1 (PP1) that is at

the end of the Pixel Support Tube.

A schematic overview of the pixel electrical and optical services is given in Figure 3.

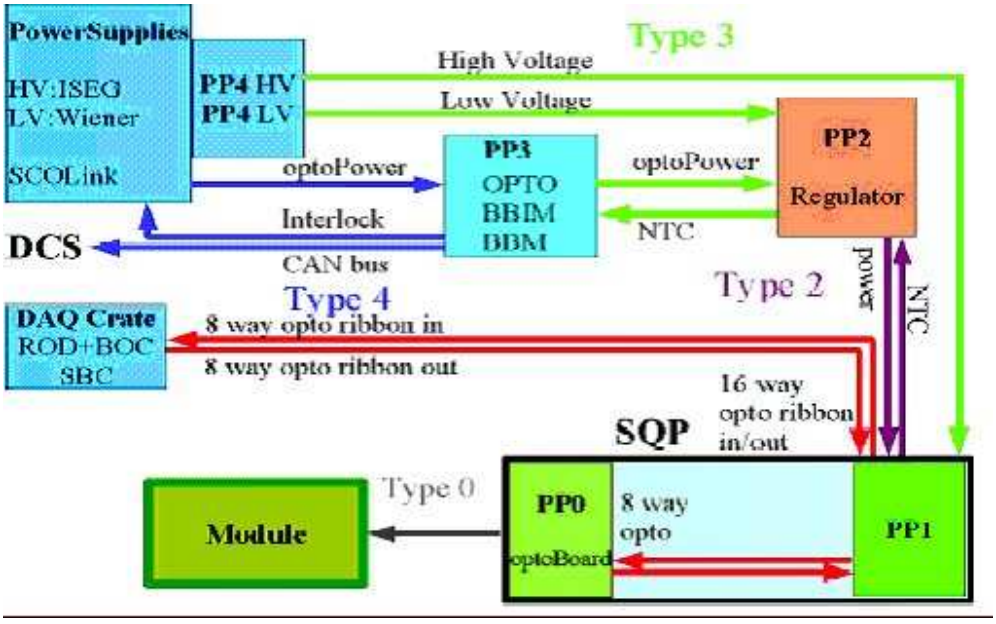

Figure 3. Schematic of the pixel electrical and optical services.

Optical transceivers (optoboards) are located on the SQPs (see Section 4.4 for a description of the optical system). Power for the pixel modules is supplied by power supplies located in the ATLAS services caverns [Ref] and is regulated at the Patch Panel 2 (PP2) location. High voltage is supplied by power supplies in the service caverns. Routing of low voltages and high voltages occurs at the Patch Panel 4 (PP4) region. Monitoring (and power distribution for the optical items) occurs at the Patch Panel 3 (PP3) region. Internal services (those within the Pixel Support Tube) are described in section 7.4. External services are described in section 7.5.

Cooling connections are also made at PP0 and at PP1. Individual heat exchangers for each pixel cooling circuit are embedded in the Service Quarter Panels. The heater exchangers and these connections are described briefly below in section 7.4. A general description of the ATLAS evaporative cooling system may be found in [Ref].

3. Barrel Region

The pixel detector barrel region (see Figure 4) has three concentric layers with modules loaded on local supports (staves) supported by three shells. The global support described in section 1 surrounds the shells and supports them through four radial fingers at the ends of the barrel region. Each stave [**?**] is about 800 mm long and carries 13 pixel modules tilted in both the Z-R and R-Φ planes by 1.1° and 20°, respectively. There are in total 112 staves. Two staves share a single cooling loop generating an assembly called a bi-stave with 26 modules. The modules are distributed over the three layers as summarised in Table 1.

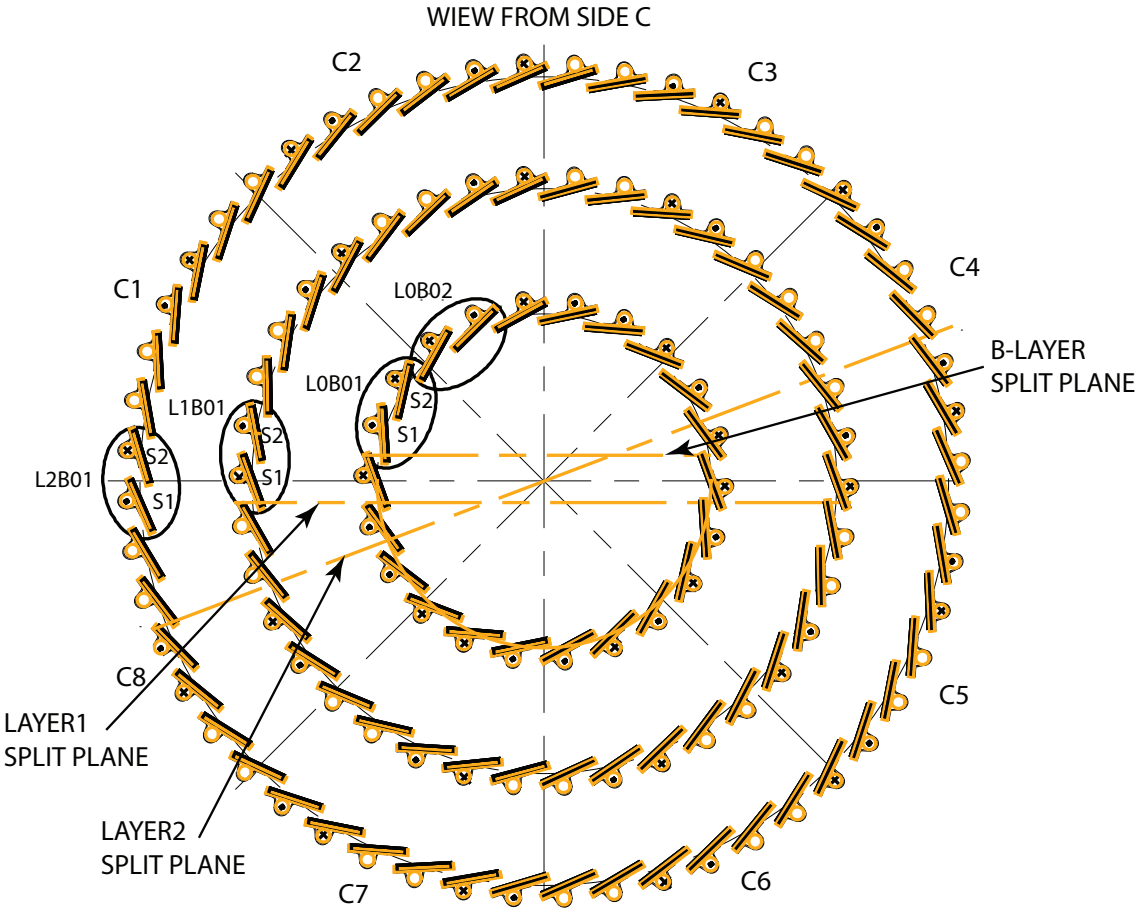

Figure 4. Layout of the Pixel barrel region. Support shells are not shown.

	B-layer	Layer 2	Layer 1	Total
Average radius [mm]	50.5	122.5	88.5	
No. of bi-staves	11	26	19	56
No. of staves	22	52	38	112
No. of modules	286	676	494	1456
No. of pixels	$1.317 \cdot 10^7$	$3.115 \cdot 10^7$	$2.276 \cdot 10^7$	$6.709 \cdot 10^7$

Table 1. Parameters of the pixel barrel region.

3.1 Staves

A stave is an assembly of three parts (see Figure 5): a Thermal Management Tile (TMT); the omega piece; and the cooling pipe. The TMT is machined out of a Carbon-Carbon (C-C) plate yielding a series of 12 shingled steps symmetrically placed (6 each side) around a central flat step. The shingled geometry allows for an overlap between the 13 modules mounted on the stave, to achieve hermetic coverage. The C-C material has been adopted for many reasons:

- good transverse thermal conductivity, adequate for an efficient heat transfer from the surface

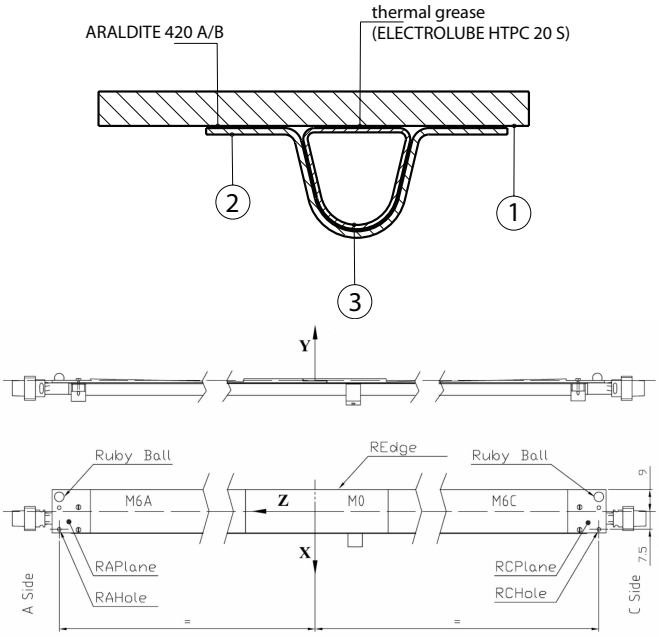

Figure 5. (a) top, cross section of a stave. Part 1 is the TMT, 2 is the omega piece and 3 the aluminum pipe. (b) bottom, longitudinal views of the stave with the reference system used for survey.

to the cooling channel;

- low radiation length;
- excellent stiffness and stability;
- low value (close to zero) of the coefficient of thermal expansion (CTE).

The omega piece is made of three layers of unidirectional, ultra-high modulus carbon fiber, with cyanate ester resin. The lay-up (0-90-0) is 0.3 mm thick and has been optimized through an extensive design and test program. The choice of the material and of the lay-up has been done in order to achieve a longitudinal CTE as close as possible to the CTE of the C-C TMT, to minimize distortions due to cool down of the structure. The omega-TMT-longitudinal CTE mismatch, less than 1 ppm, allows the stave to meet the stability requirements. The omega is bonded to the TMT using an adhesive[1] featuring a high peeling strength.

A D-shaped (see part 3 in Figure 5) aluminum pipe, with a 0.3 mm thick wall, is located in the TMT/Omega structure. It provides the cooling channel for the C_3F_8 coolant. The aluminium tube is made of a 6061 Al-alloy, precisely shaped by extrusion to fit inside the omega piece with a clearance of 50 μm. The tube hydraulic diameter is 4.15 mm, which allows cooling of two staves in series with an acceptable pressure drop. A pressure drop of about 50 mbar over one stave has been measured during the thermal tests. Thermal grease[2] is used to fill the gap between the tube

[1] CIBA Araldite® 420 A/B, from Huntsman, former Ciba Specialty Chemicals (www.huntsman.com)

[2] HPGP thermal grease from Electrolube (www.electrolube.com).

and the TMT. Use of this grease interface reduces the mechanical coupling between the tube and the C-C. This minimizes the stave distortion from cool down.

During the production of staves, several problems were encountered that caused a change in the design and fabrication. The original design had the ends of the aluminium pipe coated with nickel, by an electroless process, in order to attach aluminium fittings by brazing. Staves, before and after modules were loaded, went through a qualification process that used an aqueous solution as a coolant. The presence of water triggered a corrosion process in the aluminium pipes. The corrosion was due to a galvanic process where water and traces of halogen (like Cl) acted as an electrolyte. The effect of the galvanic corrosion led in some cases to holes in the pipe, as may be seen in Figure 6.

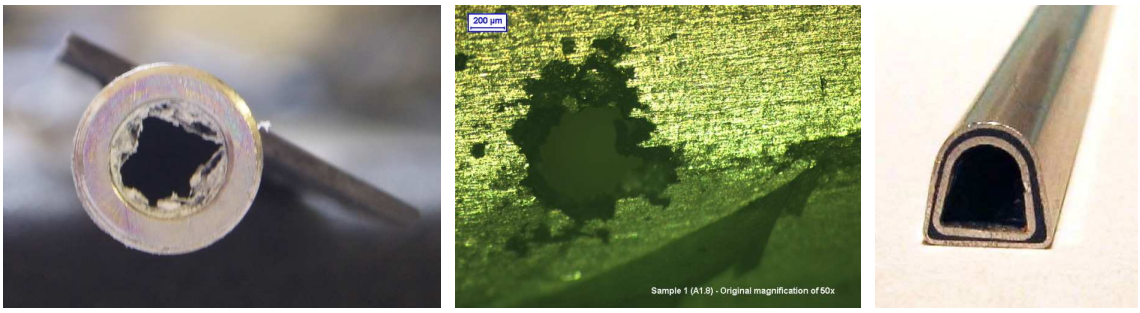

Figure 6. On the left, a view of the end of the stave pipe after corrosion. The nickel layer is detached from the aluminum by the formation of aluminum oxides. The picture in the centre shows a detail of the pipe with a through hole. On the right, a picture of an inserted pipe to recover staves already loaded with modules.

A significant number of staves had already been loaded with modules when this problem was found. The solution that was implemented was to insert a new pipe into the existing one. The inserted pipe (see Figure 6) a smaller hydraulic diameter that significantly increased the pressure drop along the pipe. Since the evaporation temperature depends on the pressure, there is a difference in the temperature (ΔT) between the first (higher T) and last (lower T) module of a stave, and this difference was increased for a smaller hydraulic diameter.

The thermal impedance from the coolant to the TMT is also increased for two pipes. There is a 150 μm gap between the two pipes, filled with an alumina loaded epoxy[3] having a thermal conductivity of 1.1 W/mK. The ΔT increase is $\sim 4^{\circ}$C .

The new pipe was electrically insulated from the original one in order to protect against existing galvanic corrosion at the surface of the external pipe. Hard anodization with an oxide layer of about 30 μm of the inserted pipe was used.

The stave pipe was connected to a cooling system to verify the thermal properties. This connection applied forces to the stave pipe that were transferred to the omega piece, causing delamination the bond between the omega and the TMT. The bond quality was found to be poor because carbon powder from the C-C prevented good adhesion. The bond failure degraded significantly the thermal integrity of the grease layer between the pipe and the TMT. A dedicated inspection performed after the full production showed that more than 5 % of the staves were already delam-

[3] STYCAST 2850 FT from Emerson & Cuming (www.emersoncuming.com)

inated at the fitting area and two of them where already loaded with modules.To prevent further delamination, a glass-filled PEEK collar was added to all the staves that were used in the detector.

The failure modes (corrosion and delamination) led us to develop a recovery plan for the staves already loaded with the modules and for the ones still to be loaded. The recovery plan from corrosion followed three different paths:

1. Insertion of a new aluminium D-shaped pipe into the corroded pipe. Tests performed with an evaporative cooling system have shown that modules of such bi-staves run above 0 °C. Results are reported in Table 2.

2. Fitting were attached to all pipes by laser welding, thereby eliminating eliminating brazing.Bare staves (staves without modules loaded) were disassembled. The old pipe was removed and replaced with one with laser-welded fittings and reassembled with a yield of about 85%.

3. A new batch of staves was produced to compensate for the losses of the refurbished bare staves.

Bi-stave type	Stave type	Measured[4]	
		Mean T	Max T
Repaired Bi-stave	Stave 1 (inserted)	$+3.3^\circ$ C	$+10^\circ$ C
	Stave 2 (clean)	-4.46° C	-0.5° C
Standard Bi-stave	Stave 1	-3.92° C	$+1^\circ$ C
	Stave 2	-5.61° C	0° C

Table 2. Estimated and measured temperature for different bi-staves. Stave 1 is upstream and Stave 2 is downstream in the cooling loop.

The barrel detector was assembled with a mixture of three different type staves. Table 3 shows how the stave types were assigned to the three layers

Type	Comments	Layer 2	Layer 1	B-Layer	Total
Inserted staves Pipe inserted (1)	26	0	0	26	
New Staves New pipes (2)	2	15	11	28	
Repaired Staves Pipe substituted (3)	24	23	11	58	

Table 3. Distribution of the different types of staves in the barrel layers.

3.2 Barrel Module Mounting

Modules mounting on staves started in the summer of 2004 to verify procedures. There were three module-loading sites. After qualification of all three sites, production continued at full speed until the corroded aluminum pipes in staves were discovered. This problem stopped module loading for six months. Once new staves were available, module loading was immediately restarted and later continued in parallel with bare stave production. The last stave was assembled in October 2007.

The loading procedure and the qualification tests are described in the following paragraphs. Stave loading was done using specially designed robots in a semi-automatic way by trained operators. Three module loading robots were installed: sites 1 and 2 had similar designs (shown in Figure 7), while site 3 had a different one [**?**]. All setups were located in clean rooms with temperature control.

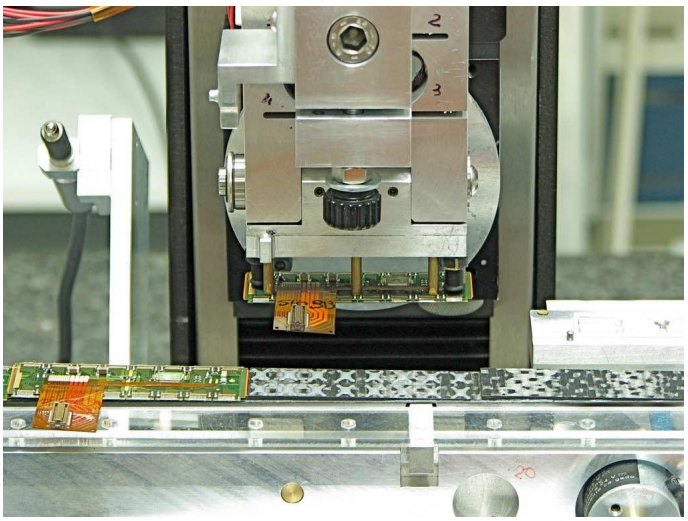

Figure 7. Loading robot used in sites 1 and 2. Blow up of the module pick-up head.

Detector modules had to be fixed with a precision better than 50 μm in both directions on the stave plane. Nominal module positions were defined in a stave reference coordinate system constructed individually for each stave based on stave reference points (machined edges, tile steps and reference planes on stave ends). Some of these reference points are inaccessible after stave loading, so to control the module positions and to translate these positions to the global ATLAS coordinate frame, two precision ruby balls were mounted on each stave. Together with the reference planes, they allow the measurement of module positions.

The determination of the stave reference frame and the survey of module positions after stave loading was done with a coordinate measuring machine (CMM) with mechanical, optical and laser probes at sites 1 and 2. Site 3 used a specially designed optical system connected with the loading robot. The single point measurement precision was between 5 and 10 μm for contact probes and between 5 and 20 μm for optical probes depending on the surface quality. Several measured points were averaged to improve accuracy.

Loading started with a determination of the stave reference system. The stave was fixed on a moving trolley (sites 1 and 2) or granite table (site 3) to guarantee precise placement of the modules by the loading robot. To guarantee uniform cooling, a gap between a pixel module and the stave surface must be constant ($\sim$100 μm) everywhere. Due to the shingled-stave design, modules are inclined by $\sim$1.10° before gluing. The ideal position of a pixel module located 100 μm above the stave surface was stored in the robot memory and module was moved away to allow glue deposition.

A thermal-conducting, flexible epoxy glue [5] was used to fix modules. After glue deposition, a module was returned by the robot to its predefined position 100 μm above stave surface and left in this position until the glue cured. The force holding the module was adjusted to control the quality of module-stave joint.

A loaded stave was surveyed on a CMM. Deformation of pixel modules (bow) was measured using different methods. All measurements were taken with respect to the two ruby balls mounted on each stave. The deviation of modules position from nominal in X (transverse to the stave axis) and Z (along the stave axis) coordinates are shown in Figure 8 [**?**]. Only a few modules have deviations bigger than 50 μm.

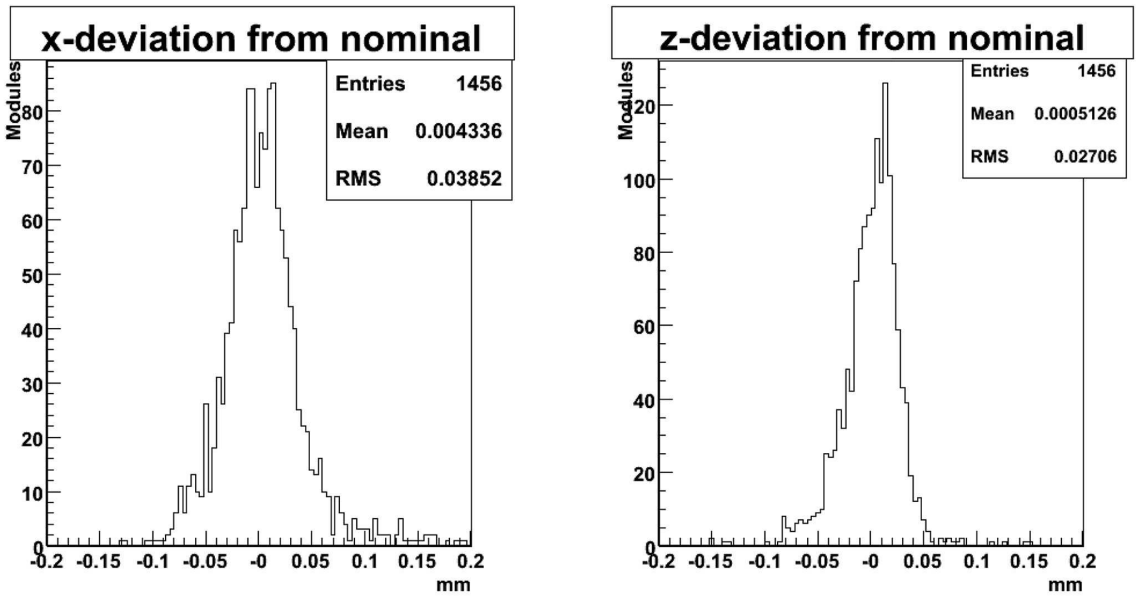

Figure 8. Deviation of module positions from nominal values for the barrel modules as described in the text.

The fully-loaded staves under to measure a characterization procedure to test the modules after the loading as well as to measure the thermal performance of the assembly. The testing sequence was similar to the one used to qualify modules individually. The testing sequence was as follows:

- module configuration, measurement of threshold dispersion and noise, threshold scan without bias to check for disconnected pixels and a sensor bias I-V scan to check the integrity of the sensor at room temperature;
- ten thermal cycles between -30°C and 30°C with a cycle time of 2 hours;
- the same tests as performed at room temperature but at about -8°C with the addition of a radioactive-source scan for the identification of disconnected pixels. The thermal performance was also obtained.

[5] Toray Silicone SE4445CV A&B, from Dow Corning (www.dowcorning.com)

A ranking function of the measured parameters was constructed to determine the stave quality and to select the staves for a particular layer. The best staves went into the B-layer. Staves with an inserted pipe were only used in Layer 2 (Table 2).

3.3 Half-shells

The barrel shells (see Figure 9) were constructed from two half-shells. Bi-staves were attached to a half-shell. Ten aluminium-alloy fasteners screw each bi-stave to support rings bonded to a shell. All the shells are supported off the end-cones of the pixel support frame (Section 8.l) PEEK elements are bonded at both ends of the half-shell to provide the interface to the fingers of the end-cones. Shells were made from carbon-fiber-reinforced material. A quasi-isotropic laminate made

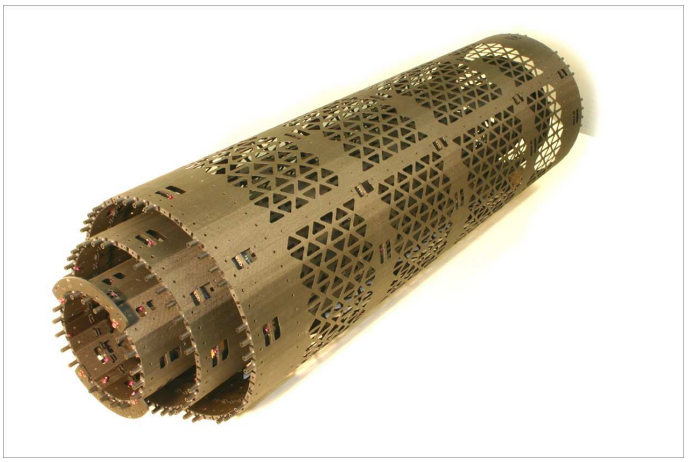

Figure 9. Picture of the three barrel shells

of six plies $(0^\circ/60^\circ/-60^\circ)$ of unidirectional ultra-high-modulus carbon fiber[6]/cyanate-ester[7] was made. The shells are not cylinders, but have flat surfaces locally. The overall mass was reduced by cutting out material in each shell, as show in Figure 9.

The accuracy of the interface to a stave was set to be better than 50 μm. The maximum gravity deflection of each assembly was designed to be less than 50 μm. Table 4 shows results from a survey done on the as-built assembly. The values reported in the table are the maximum deviations observed over several hundred data points taken all over the structures. The large majority of them ($> 90\%$) are within the specifications.

3.4 Bi-stave Integration and Half-shell Loading

Two staves (see Figure 10), each loaded with 13 pixel modules, were assembled together. Type 0 cables (section 8.5) were connected to the module and properly routed along the staves. Electrical testing was done during bi-stave assembly as was leak checking of the two cooling loops after connection of a U-link (section 8.5)

[6]Carbon fiber YS80, from Nippon Graphite Fiber Corporation (NGF) (http://www31.ocn.ne.jp/ ngf/english/)

[7]EX-1515 Cyanate Ester resin system, from TenCate Advanced Composites, former Bryte Technologies Inc (www.brytetech.com)

	Shell Accuracy [μm]			
	Requirements		As built	
	All Layers	Layer 2	Layer 1	B-Layer
Geometrical accuracy	50	70	62	55
Gravity sag	50	98	68	80

Table 4. Comparison between the geometrical design requirements and the maximum deviations from an ideal geometry as surveyed.

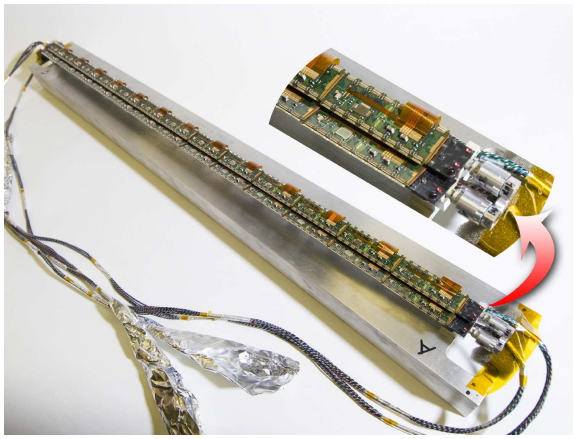

Figure 10. A bi-stave assembly.

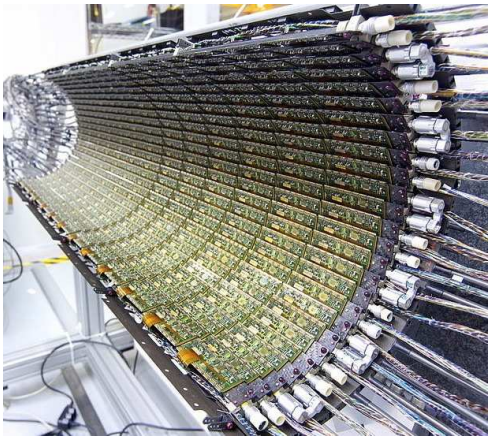

Figure 11. Layer 2 half-shells with all the bi-staves installed.

Bi-staves were integrated by hand into the half-shells starting with Layer 2 and proceeding to the B-Layer. Figure 11 shows one of two half-shells with all the bi-staves installed for Layer 2.

Once the bi-stave loading was completed, the half-shells underwent a geometrical survey. The stave reference points provided by two ruby balls glued at the ends of each stave were surveyed with respect to the half-shell reference points. Although the module position is known in Z with a typical accuracy of about 10 μm, the inaccuracy in Φ and in R is significantly worse. The stave can

bow in a half-shell during attachment up to 200 μm in Φ at the central support (Z=0). The effects on individual modules could not be determined because modules could not be surveyed directly on a half-shell.

3.5 Half-shell Clamping

Two half-shells of each layer were clamped together into a complete shell. A half-shell lacks torsional stiffness (around the axis of the cylinder). Half-shells were stiffened with an external structure and kept undeformed during the integration process. The shell transferring tool (STT) held each of the two half-shells by ten clamps that grabbed each half-ring in two places. The tool was placed on the flat surface of a granite table that provided the reference plane. The bottom half-shell is kept on the STT and the top one was lowered until it engaged the clamping features (see Figure 12).

Figure 12. Clamping of the Layer 2 half-shells. The top half is craned onto the bottom one resting on the STT (see text). The picture shows the mechanism that guides the process. The stainless steel pipe, visible along the the axis of the shell, was used to guide the insertion into the global frame and was removed afterward.

The operation was delicate due to the fact that the wire bonds of the modules were exposed and clearances were about 1mm. Once the half-shells are joined, they can be removed from the STT. The load of the shell was taken by the metal pipe passing through the shell and visible in Figure 12. Figure 13 shows the Layer 2 shell clamped and moved onto the integration and testing tool (ITT) for integration into the global support frame (section 8.6). Layer 1 followed the same clamping procedure. The B-layer required a more complex procedure. The flanges at the extremities of the beam pipe do not pass through the B-Layer and it has to be clamped around them (Section 8.6). More details of the assembly and testing procedures can be found in [**?**].

4. Endcap Region

The active elements of the pixel detector in the two endcap regions are disk sectors, each supporting six modules (three on each side). Eight disk sectors are supported on a disk support ring, forming a disk. There are three disks in each of the two endcaps. The disks in the endcaps are rigidly held

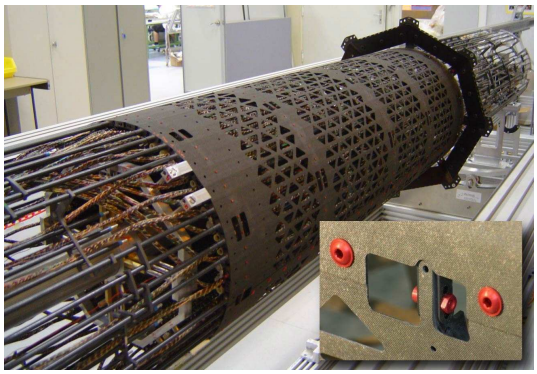

Figure 13. Layer 2 clamped and resting on the axis of the ITT before being inserted into the global frame.

by the global support frame. This section will describe the construction, survey and testing of the disk sectors (8.3.1), disks (8.3.2) and endcaps (8.3.3).

4.1 Disk Sectors

Construction

The local support structures (with integrated cooling) for the modules in the endcap region are called disk sectors. The sectors are roughly trapezoidal in shape, and consist of two thin carbon-carbon sheets with a rectangular aluminum cooling tube and carbon foam in between the sheets. The cooling tube is bent into a W-like shape to fit within the sector, and makes contact with the carbon-carbon sheets with a compliant, thermally conducting adhesive. Each cooling circuit in the disk region serves two sectors.

The carbon-carbon material was manufactured in large panels approximately 50 cm x 50 cm [**?**]. The faceplates of the sectors were precisely machined from pieces rough cut from the large panels. The thickness of each sector faceplate was measured and the average thickness was 0.42 +/- 0.024(rms) mm. Carbon foam of density about 0.09 g/cc was glued (using a cyanate-ester-based film adhesive) to one faceplate and a slot machined for the aluminum tube [**?**]. The rectangular aluminum tubes were bent into a precise shape and work-hardened to increase the resistance against deflection from internal pressure [**?**]. All tubes were conformally coated with an insulating material(thickness of about 12 μm) to prevent direct contact between the tube and the carbon-carbon faceplates [**?**]. The tubes were attached to the faceplates with a compliant thermal adhesive [**?**].

Extensive quality control was implemented during the fabrication of the sectors. The overall thickness of each sector was measured in multiple locations. The nominal thickness was about 3.32 mm. The thickness variation within a sector was less than 50 microns, typically within 25 microns. The weight of a sector was about 27.3 g with a variation of less than 2

Three modules are mounted on each side of the sector, with the long dimension of the module in the radial direction. The three modules on the back of the sector are rotated 7.5 degrees with respect to the modules on the front side, thus providing full overlapping azimuthal coverage. Figure 14 shows three modules mounted on the front side of a sector.

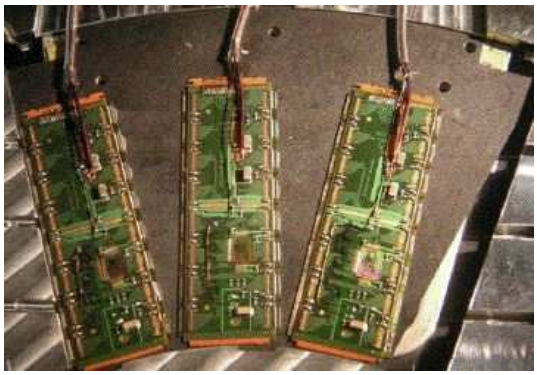

Figure 14. Three endcap pixel modules mounted on the front side of a sector.

The modules were glued to the sectors with Dow Corning silicone SE4445. Nylon filaments of 110 μm diameter are used to control the silicone thickness. The positions of survey targets in the corners of each module were viewed with an optical coordinating measuring machine during the gluing operation. The modules were positioned initially using precision tooling. Final adjustments were made by hand while viewing the targets using the optical instrument to position a module as close as possible to the nominal position. The optical measuring machine had an intrinsic accuracy of better than 2 μm in the module plane and about 5 μm in the plane perpendicular to a module.

Sector Survey

After the modules were glued to the carbon-carbon surface of the disk sectors, the sector was again mounted on the table of an optical CMM. The CMM very precisely measured X,Y coordinates (in the plane of the sector) by measuring the position of the CMM table, and measured Z coordinates (perpendicular to the sector) with optical focusing. The X,Y positions of survey targets at the four corners of modules mounted on a disk sector were measured, and these measurements are used to determine the position and orientation of the module in the plane of the sector. The CMM also measured 32 X,Y,Z points on the top side of modules mounted on a sector (16 along one long edge, 16 along the other long edge) in the vicinity of the first and last chip ID pads of each front-end chip, and these measurements are used to determine the position and rotations of the module out of the sector plane. The pixel module is treated as a flat rigid plane, as the module distortions (such as bow) were measured to be very small, well below values that would impact tracking resolution in the disk region.

The alignment parameters of each module were calculated in the local module reference frame from these measurements. The module alignment parameters are those 6 parameters used to describe a flat plane: X, Y, Z, Φ_x, Φ_y, Φ_z. X is the coordinate across the short width of the module, and Y is the coordinate along the long length of the module. In the local module reference frame, the module alignment parameters are the displacements of the module from its nominal position (i.e. the difference from nominal). The X,Y,Φ_z alignment parameters calculated from the sector surveys are not the final survey alignment parameters, as they do not include the effect of the placement of

the sector on the disk ring. Details about the calculation of the module alignment parameters are given in [**?**].

In Figure **??** the distributions of the X,Y,Φ_z module alignment parameters calculated from the sector surveys are given(treating all the modules as A-side modules, which means plotting the negative of the actual X and Φ_z values for the C-side modules). The means and sigmas of the Gaussian fits to these distributions are given in Table **??**. One sees several features:

- The mean of the X alignment parameter distribution is different for front and back modules: -2.8 μm for front modules, and $+2.8$ μm for back modules. This is due to a small systematic offset when the modules were mounted on the sectors. The opposite sign occurs when converting the survey measurements to the same coordinate system.

- The average sigma for the X and Y alignment parameter distributions is 2.0 μm, and the sigma for the Φ_z alignment parameter distribution is 0.064 mrad. These resolutions include both the placement accuracy and the measurement precision, and thus represent upper limits on the placement accuracy. These small values show that the modules have been placed on the sectors with excellent accuracy of better than 2 μm.

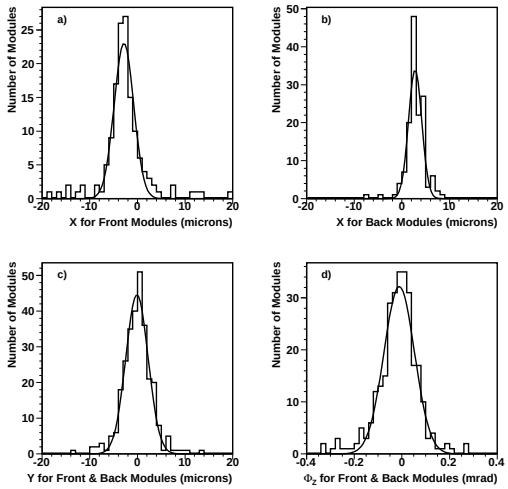

Figure 15. X,Y,Φ_z alignment parameters calculated from the sector surveys.

	Mean	Sigma
X for Front Modules	-2.8 ± 0.2 μm	2.1 ± 0.2 μm
X for Back Modules	$+2.8 \pm 0.1$ μm	1.4 ± 0.1 μm
Y for Front and Back Modules	-0.1 ± 0.1 μm	2.3 ± 0.1 μm
Φ_z for Front and Back Modules	-0.011 ± 0.004 mrad	0.064 ± 0.004 mrad

Table 5. Results of the Gaussian fits to the sector survey distributions in Figure **??**.

Sector Testing

Electrical and thermal tests were performed on the modules after they are glued onto the sectors. The goal is to check any degradation of module performances (early breakdown, increased noise, bump failures, etc.) caused by thermal or mechanical stresses from loading. Another aim is to rank the sectors for disk loading so that the sectors with the least number of bad pixels can be loaded onto the innermost disks. The tests performed on each module are part of the full quality control procedure of the ATLAS Pixel Detector and more details are given in [**?**]. The electrical sector testing sequence consists of the following three sets of basic monitoring scans:

- LOAD test: This test is performed immediately after sector loading at room temperature. The test includes I-V, digital, analog threshold, crosstalk and source scans. Data from this test are compared to the single module BURN test (a test performed under similar conditions before the module was loaded on the sector) to observe any changes due to sector loading. All six modules on the sector are tested individually before proceeding to the next test.

- INBURN test: During this test the sector is cold soaked for a period of about 12 hours at -30°C with the power off. It is then thermal cycled between -20°C and 20°C (T_{NTC}=-16 to 25°C) with the power on. The dwell time at each endpoint is 1 hour and the entire test consists of 14 cycles with about 3.5 hours per cycle. Digital and analog threshold scans are run throughout the burn-in, while monitoring T_{NTC} and digital/analog voltages and currents.

- STAVE test: The full electrical characterization is performed after burn-in at operating temperature (T_{NTC}= -5 to -10°C) for a fully configured module. The test includes all LOAD scans as well as MonLeak, in-time threshold and GDAC scans. Data from this test are compared to the single module FLEX test to detect any changes due to sector loading or sector burn-in, and serve as the basis for sector ranking.

Electrical testing and burn-in were performed using one setup. The details of the technical description are given in [**?**]. The standard module testing hardware chain was used: a PC computer with VME and GPIB interfaces (control cards), ATLAS Pixel TurboDAQ software, a VME crate with a custom board (ATLAS Turbo Pixel Low Level card), an external custom board (ATLAS Turbo Pixel Control Card), GPIB controlled off-the-shelf power supplies, and a LBNL custom designed SURF board with module(s) attached to it. Two surf boards [**?**] were used to connect all six modules at once. The sector was cooled using an inert flourocarbon C_6F_{14} running in a secondary loop connected to the sector cooling pipes. Dynalene (HC-50) was used in the primary loop and was cooled using a chiller. The two loops made thermal contact inside a coiled heat exchanger.

The following measurements made during the electrical tests described above were used to rank the sectors: bias current at 150 V, number of bad pixels in digital scans, number of bad pixels in analog threshold scans, number of bad pixels in crosstalk scans, number of bad pixels in in-time scans, number of bad pixels due to bump discontinuity, number of dead or masked pixels measured during source scans, threshold dispersion, and average noise.

The cuts for bad pixels are defined according to guidelines from the ATLAS Pixel Detector collaboration. The above quantities were entered into the Pixel DataBase to maintain a comlete record

of the production sequence and allow the possiblity of tracing any eventual problems. Sector evaluation also considered results from the alignment survey and thermal performance measurements during the electrical tests.

The total number of bad pixels in each of the endcaps can be estimated using the results of the STAVE test performed at the sector level since this is the last, full electrical characterization performed on the modules at operating temperature. It is also the last source scan where bump discontinuity can be accurately measured. Table **??** shows the total number of bad pixels for each of the endcaps, classified by failure. Bad pixels are not double counted: if a pixel is bad digitally, it is not counted as analog bad or source bad.

EndCap	SOURCE	MASK	DIG	ANA	DISC	XTALK	INTIME	TOTAL	%
A	5497	373	5816	471	2559	171	2671	17531	0.26
C	4221	360	52	594	636	127	3131	9036	0.14

Table 6. *Number of bad pixels for each endcap, classified by failure. Results are taken from the STAVE test and later connectivity tests.*

4.2 Endcap Disks

8.3.2.1 Construction

Eight disk sectors are mounted on a 312 mm diameter carbon composite disk support ring, forming a disk. There are three disks in each of the two Endcaps. Each disk has 48 modules, for a total of 288 modules. The radius of the module centers is approximately 119 mm. The inner radius of the active area of the pixel modules is approximately 89 mm. Figure **??** shows one of the completed disks.

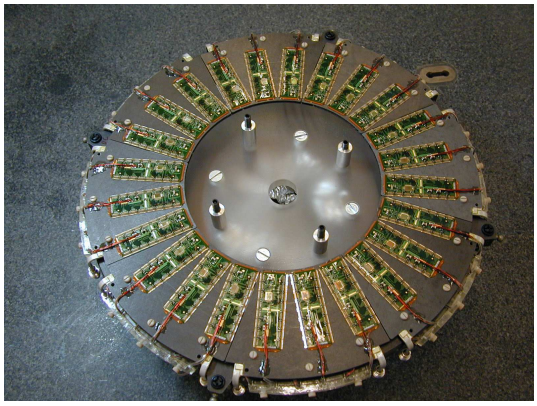

Figure 16. Eight sectors assembled into a disk.

8.3.2.2 Disk Survey

After the disk sectors are mounted on the disk ring, the X,Y positions of the survey targets at the four corners of each front module are again precisely measured with the SmartScope, and are used to determine the final survey position and orientation of the front modules on the disk with a precision of a micron. The back modules are not surveyed after mounting the sectors on the disk, but the measurements done after mounting the modules on the sectors are used to calculate the positions of the back modules on the disks with a precision of about 5 microns.

The final X,Y,Φ_z alignment parameters of the modules were calculated from the disk survey SmartScope measurements in a manner similar to the way they were previously calculated for the sector survey measurements. These final X,Y,Φ_z alignment parameters are the displacements from nominal due to both the placement of the modules on the sector and the placement of the sectors on the disk ring.

In Figure **??** are the distributions of the final X,Y,Φ_z module alignment parameters calculated from the disk surveys (treating all the modules as A Disk modules, which means plotting the negative of the actual X and Φ_z values for the C Disk modules), and in Table **??** are the means and sigmas of the Gaussian fits to these distributions. One sees several features:

- The average sigma for the X and Y alignment parameter distributions is 12 μm, and the sigma for the Φ_z alignment parameter distribution is 0.130 mrad. These values include both the placement of the modules on the sector and the placement of the sectors on the disk ring. Recall from the sector survey results (which only include the placement of the modules on the sector), that the average sigma for X and Y was 2.0 μm, and the sigma for Φ_z was 0.064 mrad. Thus we see a much larger variation in the module position due to the sectors being placed on the disk ring than due to the modules being placed on the sector.

- The mean of the Y alignment parameter distribution is 35 μm. The local module Y direction is the radial direction in the disk. The reason that the Y alignment parameter is so large is mostly because the average radius of the mounting holes in the disk rings is larger than the nominal value of 156 mm. From independent disk ring measurements, the radius appears to be roughly 25 μm larger than nominal. This accounts for the major part of the 35 μm.

	Mean	Sigma
X for Front Modules	-0.1 ± 1.1 μm	12.6 ± 0.9 μm
X for Back Modules	1.1 ± 1.0 μm	11.5 ± 0.8 μm
Y for Front and Back Modules	35.3 ± 0.7 μm	11.4 ± 0.6 μm
Φ_z for Front and Back Modules	-0.029 ± 0.008 mrad	0.130 ± 0.009 mrad

Table 7. Results of the Gaussian fits to the disk survey distributions in Figure **??**.

8.3.2.3 Disk Testing

After the sectors were mounted on a disk ring, a continuity test was performed on the modules. Its purpose was to quickly check that the delicate module circuitry survived the mounting operation

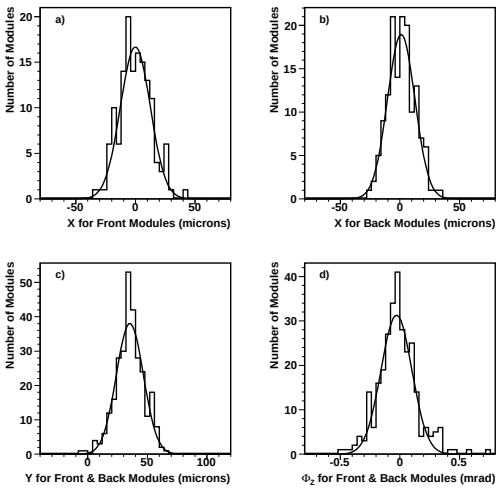

Figure 17. Final X,Y,Φ_z alignment parameters calculated from the disk surveys.

and any sector or disk handling. Since it was done without cooling, at room temperature, the modules were powered on a chip-by-chip basis, one-at-a-time, and only for a short time. The continuity test was performed as each sector was mounted on the disk ring, and again upon the disk completion. It took about 5-10 minutes per sector.

An electrical test was then done after the continuity test. The purpose of the electrical test was to check that no subtle changes occurred during the mounting of the sectors on the disk ring, and to verify the stable performance of all modules. The electrical test was a shorter version of the LOAD test done during sector testing, and it involved the following scans:

- MCC scan: This is a test of the MCC operation and connectivity.
- Digital functionality: This scan checks all registers (global and pixel front-end) and all buffers using digital injection to test full overflow conditions. It tests all pixels with digital injection (digital inject scan). This must do be done with nominal VDD voltage at 40 Mbps single link, 80 Mbps single link, 40 Mbps dual link, and 80 Mbps dual link.
- Analog functionality: This is the most time-consuming and complex set of scans performed with the bias voltage on. It is a sequence of operations and scans needed to certify proper analog behavior: threshold tune using internal injection to set a uniform threshold along the module, internal injection threshold scan (measures threshold and noise of each pixel using internal injection), FDAC tune and test, ToT tuning (tune the ToT response to a MIP signal for each pixel in order to have a uniform response to the collected charge in a time acceptable for operation in ATLAS; it calibrates the relationship between the measured ToT and collected charge), and the cross-talk scan to measure the cross-talk fraction and to detect bump defects resulting in increased capacitive coupling between pixels.
- Noise occupancy: This test consists of enabling one front-end chip at a time in self-trigger mode and measuring the rate of hits. Whereas pixels that generate hits at a rate greater than

1 Hz (1 kHz) are flagged as hot and are disabled in the slow (fast) mask during module and sector testing, it is not the case during disk testing. Here we only record their total number and compare these results with noise scans performed during sector testing.

A sensor bias voltage measurement was performed after the electrical scan was finished because we could not control the relevant power supply from the ATLAS TurboDAQ program. The bias voltage was ramped up to 600 V in 10 V increments to check for possible sensor damage. The current stability at different bias voltages was investigated over a period of more than 15 minutes.

4.3 Assembly of Disks into Endcaps

8.3.3.1 Construction

To assemble each endcap, three disks were rigidly supported by four mounts within a lightweight, octagonal, carbon composite support frame, shown in Figure **??**.

Figure **??** shows a perspective cut-away view of the pixel detector. The view shows individual barrel and endcap modules, supported with their associated services on staves and disks within the octagonal support frame.

Figure 18. Carbon composite support frames.

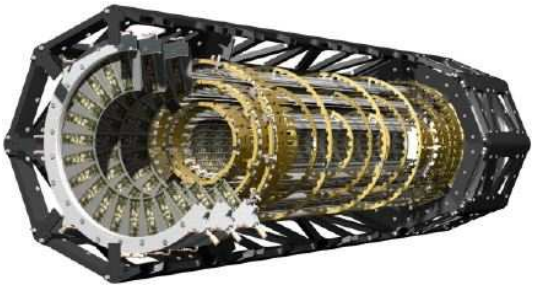

Figure 19. A perspective cut-away view of the pixel detector..

8.3.3.2 Endcap Survey

No surveys were done of the modules or sectors after the disks were assembled into an endcap, since the relevant fiducial marks were not viewable at that point.

8.3.3.3 Endcap Testing

All cooling circuits on both endcaps were leak checked down to $1-4 \times 10^{-9}$ Torr. This is the value required by the evaporative cooling system.

A connectivity test of the endcaps was performed at various stages of the integration to ensure that no modules were damaged during handling or transport. A connectivity test consists of a series of basic functionality checks performed chip-by-chip with no cooling. Each module is powered briefly and the digital, analog and bias voltages and currents are measured and compared to a set of standard values. A MCC scan is then performed as well as FE chip register/receiver tests. Each FE chip is configured to measure voltages and currents, which are compared to expected values. Finally, a short threshold scan is performed with and without bias voltage to verify that the high voltage is properly delivered to the module. The total testing time required for one endcap is two days.

A connectivity test was performed on both endcaps after loading, but before shipment to CERN.

The connectivity test was repeated after delivery of the endcaps to CERN to verify that no modules were damaged during the transport. Testing of Endcap C at CERN showed no failures on any of the modules. Endcap A showed no failures at CERN other than the three failures reported before shipment. An additional connectivity test for Endcap C was performed after integration into the Pixel Package. The test found one module with missing high voltage due to a weak bond on the module. The bond was repaired by adding silver epoxy to the high voltage hole.

Since Endcap A was used in a system test at CERN, an additional connectivity test was performed before any further integration to check for any damage to the modules during the system test or during handling in preparation for the system test. There were several modules found with intemittent HV failures. These problems were fixed by re-soldering the HV pins on the ELCO connector, by adding solder to HV wire connections, by adding silver epoxy to HV bonds, or by reinforcing glue tacks.

5. Internal Services and Support Structures

We describe in this section the internal electrical and cooling services for the pixel detector and the related support structures. Internal services (electrical, optical and cooling) are those elements within the volume of the Pixel Support Tube (see Figure 8.1.1 for an overview). The elements of

the electrical internal services are:

- Custom Type 0 cables attached to each pixel model on one end and with a miniature connector on the other;
- Patch Panel 0 (PP0) at the end of the active region of the pixel detector to which each Type 0 cable is connected via its miniature connector to a printed circuit board;
- Type 1 wire bundles that have individual wires in a bundle soldered on one end to the printed circuit boards at PP0 and feed-through printed circuit boards at Patch Panel 1 at the end of the Pixel Support Tube at the other; and

- A small number of Type 1 wires connected to temperature and other sensors.

The elements of the optical internal services are:

- Custom optical transceiver boards (optoboards, described in section 4.4) that are connected to the PP0 printed circuit boards;
- Radiation-hard optical fiber ribbons that are connected to the optoboards and to a multi-connector assembly at the PP1 region; and
- A custom optical connector at PP1.

The elements of the cooling internal services are:

- Heat exchanger assemblies for each pixel cooling loop (88 loops) that consist of inlet(warm) and outlet(cold) aluminum tubes glued together to act as a heat exchanger for the entering and exiting C_3F_8 fluid;
- Small diameter capillary tubes connected on one end to the inlet of the heat exchange and on the other to the pixel detector cooling loop or optoboard cooling loop;
- Custom shaped exhaust tubes connected on the other end of the pixel detector or optoboard cooling loop and to the outlet of the heat exchanger.

The services are held by mechanical structures within the Pixel Support Tube. There are three principal structures:

- Service Quarter Panels (SQP). There are eight total SQPs, four on each end of the detector;
- Beam Pipe Support Structure (BPSS). There is a BPSS on each side of the active pixel detector region that holds the SQPs and supports the ATLAS beryllium beam pipe. The ability to adjust the horizontal and vertical position of the beam pipe is also built into the BPSS; and
- PP1 endplate elements and associated items.

We describe below each of the elements of the internal services and associated structures. First we described the support structures to also provide an overview, then the electrical services, then the mechanical/thermal aspects of the optoboards, optical fibers and custom connector (the electrical aspects of the optoboards have been described previously in section 4.4), next the cooling services and finally the integration of the Service Quarter Panels.

5.1 Services Support Structure

The services for the active region of the pixel detector are supported by the Beam Pipe Support Structure (BPSS) on each side of the active pixel detector region as shown in Figure 8.4.1. The BPSS also supports the LHC beryllium beam pipe within the ATLAS Inner Detector region. Mechanisms to allow adjustment of the beam pipe in the plane transverse to the beam are included in the BPSS and described briefly here.

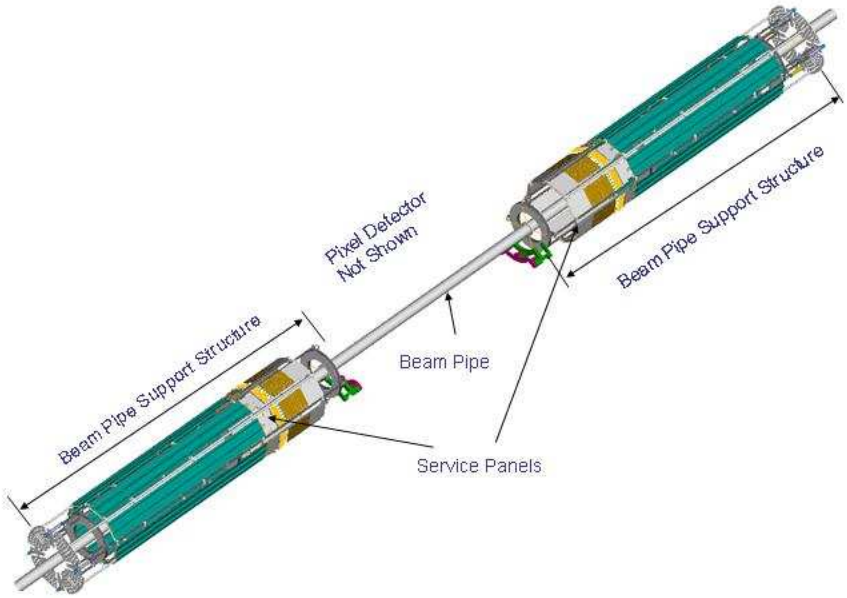

Figure 20. The relationship of the Beam Pipe Support Structure (BPSS) to the pixel detector and ATLAS beryllium beam pipe.

The BPSS is primarily constructed from carbon-fiber composite materials. The basic frame of the BPSS is illustrated in Figure 8.4.2 and consists of three, octagonal carbon-fiber-honeycomb structures with aluminum inserts that are adhesively bonded to carbon-fiber tubes to form the structure. Support points for the four service panels (see section 8.4.7) mounted on the BPSS are bonded into the octagonal structures. Supports for beam-condition monitors (Ref goes here) are also adhesively bonded to one of the octagonal structures.

Additional carbon-fiber/aluminum structures are connected to the BPSS (on an octagonal fiber/honeycomb plate) at the PP0 end to support the pixel detector support frame during insertion into the Pixel Support Tube, see Figure 8.4.3. Adjustable mount points on the pixel detector support frame ride on these structures during insertion. The precision pixel mounts bolted to an endplate on the pixel support frame engage mating mount points bonded into the PST. When this occurs, the pixel detector support frame lifts off the support structures on the BPSS by about 1 mm and is fully supported by the PST mounts. In addition, an aluminum structure is also connected at the bottom of the octagonal carbon-fiber/honeycomb plate. A cable is attached to this structure and was used to pull the pixel detector package into the Pixel Support Tube.

The adjustment of the beam pipe inside the Pixel Support Tube is implemented by attaching four stainless steel wires in an to aluminum collar in turn attached to the beam pipe at the PP0 region. The adjustment mechanism for these wires is built into the BPSS and is accessible from the end of the Pixel Support Tube after the pixel system is inserted into the PST. The adjustment range in the vertical and horizontal directions is +/-10 mm.

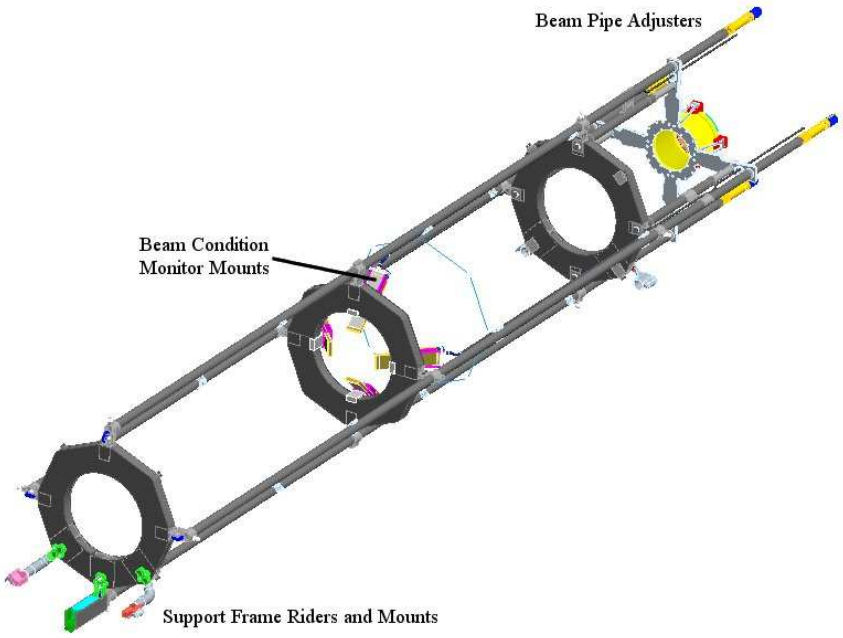

Figure 21. Illustration of the Beam Pipe Support Structure as described in the text.

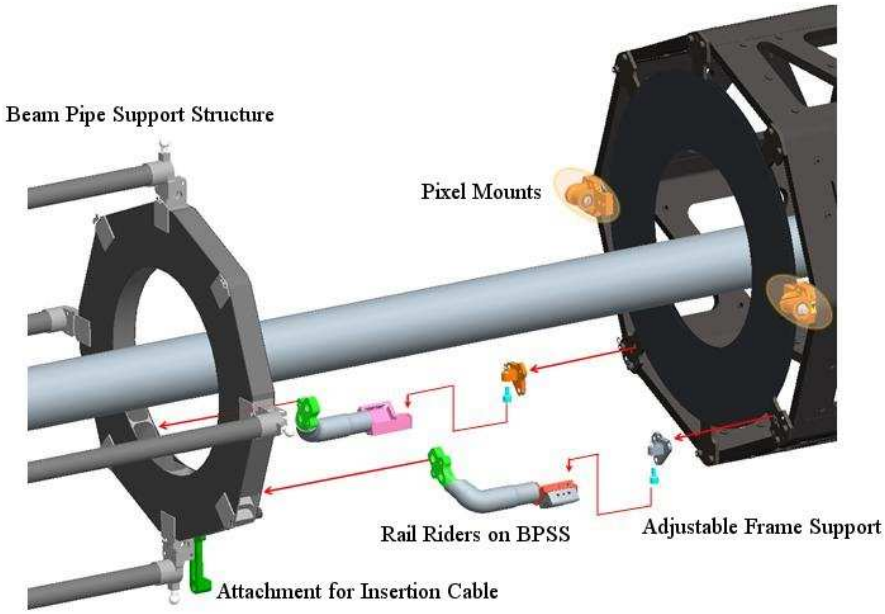

Figure 22. Expanded view of the structures on the BPPS that holdt the support frame during insertion as described in the text.

5.2 Type 0 Cables

Each module is electrically connected via a single custom, miniature, round so-called Type 0 cable. This cable consists of discrete wires terminated to a printed circuit board (PCB) housing a 36-pin, dual row, surface mount, 0.5 mm pitch connector. Type 0 cables for the barrel modules have such a connector on both ends and are connected to modules at the bi-stave integration step (section 8.2), whereas for disk cables one end was permanently soldered to the module flexible hybrid during module assembly. Each barrel module has a flexible “pigtaili" that reaches the back side of the stave, where the Type 0 cable can be plugged in. All disk 1 and 3 cables are 82 cm long, while disk 2 cables are 57 cm long, making permanent (solder) cable-to-module integration possible. However, 40 different type 0 cable lengths are required in the barrel and the length for each module is not determined before assignment of a stave to a specific position within a layer.

The barrel and disk type 0 cables are electrically similar, but the mechanical construction is different. Table 8.4.1 lists the conductors that make up each cable. All conductors have polyurethane i“magnet wire" insulation with the exception of the disk bias voltage, which has polyimide. The thickness of insulation used varies from 6 microns up to 25 microns, depending on requirements including controlled impedance of twisted pairs and high voltage hold-off for the bias voltage. All barrel conductors are pure aluminum and the termination is done by heavy-gauge wire bonding. All disk conductors have a copper exterior and are terminated by soldering. The disk current-carrying conductors are copper-clad aluminum to reduce material, and have a 90% by volume aluminum core. The material penalty from soldering and copper used in disk cables is compensated by having only one connector. The largest diameter conductor used in barrel cables is $300\mu m$ because wire bonding was not reliable for heavier gauges, thus multiple wires are used for power.

	DISK		BARREL		
Purpose	**Cond.Dia.** (μm)	**Format**	**Metal**	**Cond.Dia.**	**Format**
Analog power	400	Twisted pair	Cu-clad Al	300	6x single wire
Digital power	400	Twisted pair	Cu-clad Al	300	4x single wire
High side sense	62	Single wire	Cu	100	Single wire
Return sense	250	Single wire	Cu-clad Al	300	Single wire
Clock, data, and temp. sense	62	Twisted pair	Cu	100	Twisted pair
Bias voltage	150	Twisted pair	Cu	100	Twisted pair

Table 8. Characteristics of conductors in Barrel and Disk Type 0 cables.

The manufacture of the cables was very labor-intensive. For the disk cables, the conductors were cut to length first and then bundled manually into a silicone sleeve (surgical tubing) for protection. The individual wires were then soldered to the connector PCB and the module flex hybrid one-by-one. Figure 8.4.4a shows a section through a disk cable.

For the barrel, the bundling was automated. Spools of pre-bundled wires tied with silk thread were cut to length, processed to strip the insulation, and manually wire-bonded to the connector PCBs one-by-one. Figure 8.4.4b shows a detail of the ends of a barrel cable. The insulation strip-

ping for the barrel cables was a high temperature chemical process and this caused some problems. The geometrical arrangement of the wires during the stripping operation could result in built-in stresses that led to mechanical failure of the conductor later on. This was not discovered until a full quantity of cables for the detector had been produced. For Layers 0 and 1, new cables were manufactured with geometrical control during stripping and improved quality control. For Layer 2 enough cables were accepted from the initial production following stricter quality control, including visual inspection of the individual wires before and after mechanical stress testing.

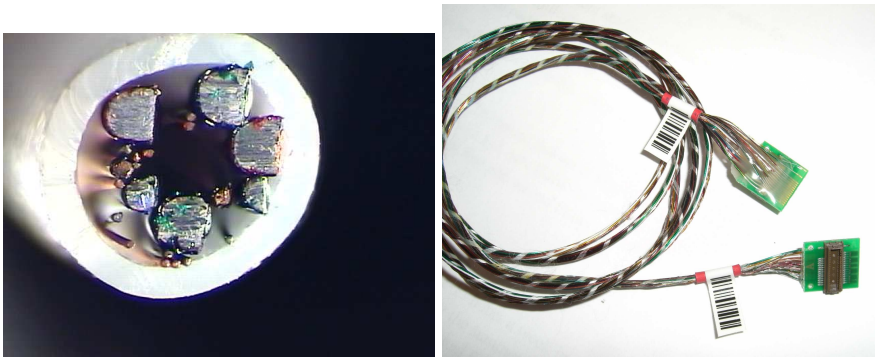

Figure 23. (a) Section through a disk T0 cable and (b) detail of a barrel T0 cable.

The voltage drops in the power conductors of the Type 0 cables are significant - approximately 10% of the total services voltage drop for just 1% of the distance. This was a conscious choice to minimize material in the detector active volume. Because of this, the resistance of each cable was carefully controlled. Figure 8.4.5 shows the measured voltage drops on the barrel Type 0 cables (this does not include the pigtail of each module which adds approximately 80mV). Figure 8.4.6 shows the distribution of voltage drops in disk cables after soldering to the module hybrid.

5.3 PP0

The Patch Panel 0 (PP0) is the first point at which the active elements of the detector are connected to the service plant. The Type-0 micro-cables with all control power and data end in one 30-pin surface mount connector at PP0. The electrical/optical conversion is made by the opto-boards that are also connected at PP0. The electrical PP0 connections are arranged on printed circuit boards. Each service panel (one panel is one octant) has one rigid printed circuit ÃćÂĂÂIJmother boardÃćÂĂÂİ housing up to 42 module connectors and 6 opto-board connectors. The core of the rigid boards is glass-filled polyimide for radiation hardness. Additionally, each outer service panel has six flexible printed circuit extensions for an additional 36 modules and six opto connectors. The flexible circuits are wrapped around the end of the panel so that these six opto boards are on the bottom of the service panel. An illustration of the PP0 region, showing elements of these printed circuit boards and other details, shown in Figure 8.4.7.

Flexible circuit boards are only used on the outer service panels. For a rigid board the opto-board is always on top (i.e. facing away from the beam pipe), whereas the flexible boards are wrapped around the end of the service panel so that their opto-boards are always on the bottom of the panel (i.e. towards the beam pipe).

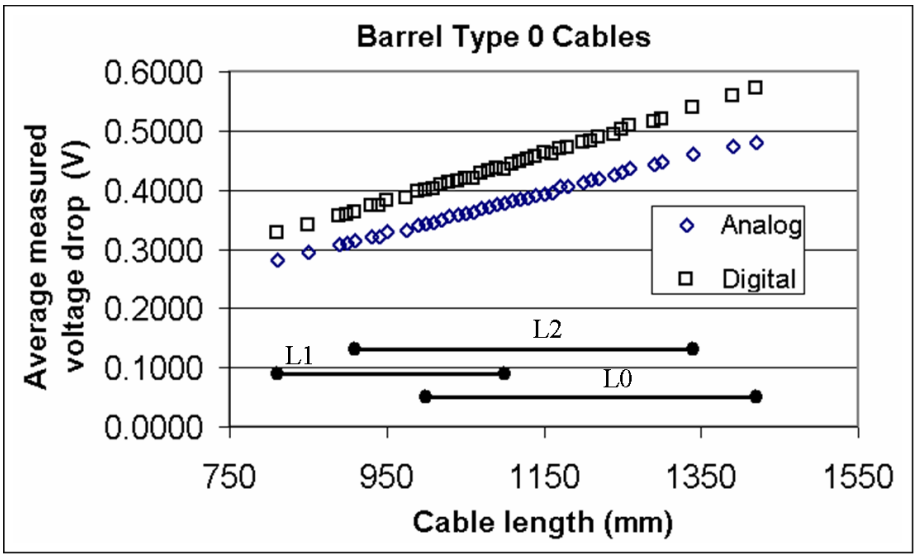

Figure 24. Average of measured voltage drops in barrel Type 0 cables vs. cable length, at the highest operating current. Values are round trip. The horizontal lines show the length range spanned by each layer. The 300-micron wire resistance derived from these measurements is 0.4 Ω/m.

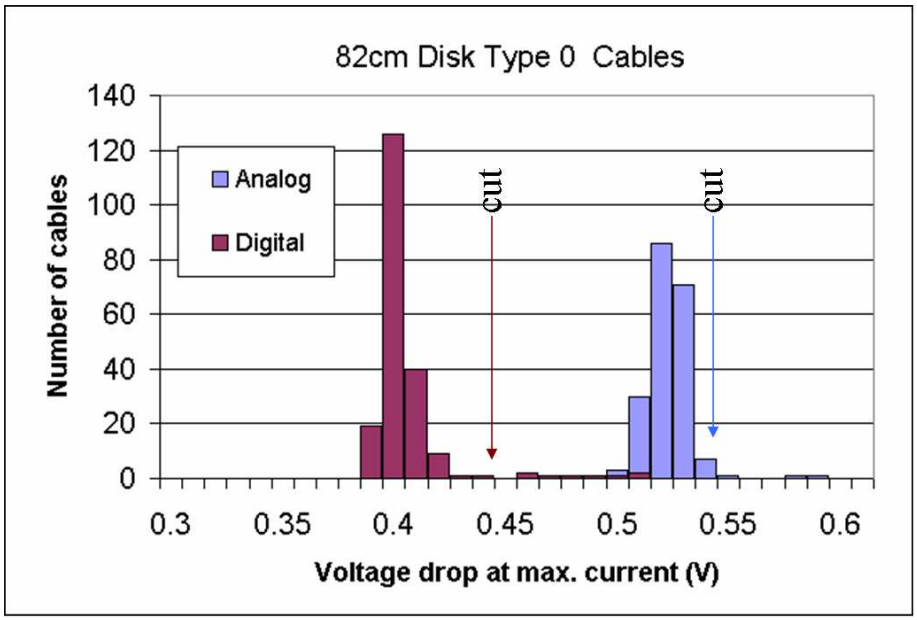

Figure 25. Measured voltage drop distributions for disk 1 and 3 type 0 cables, round-trip at highest operating current. The quality control acceptance cuts are indicated. The 400-micron copper-clad aluminum wire resistance derived from these measurements is 0.25 Ω/m.

The layout of the PP0 rigid circuit boards consists of repetitions of two basic cells, denominated PP0-A and PP0-B, which are mixed and matched at the layout level as needed. In total there
575 are five unique rigid board layouts to accommodate all the variations.

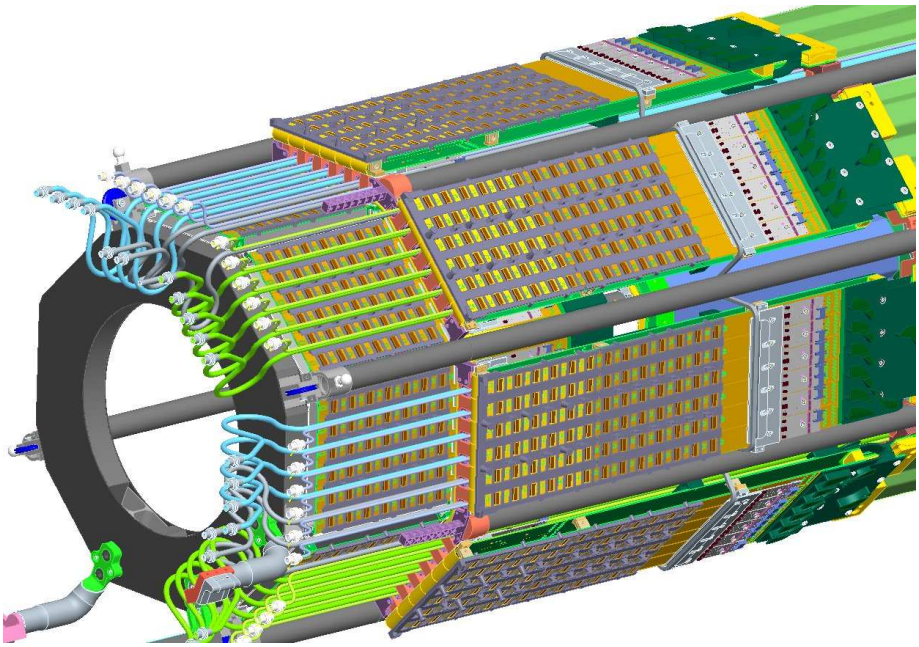

Figure 26. Illustration of the PP0 Region

Only differential signals, temperature sense lines and ground reference are routed a significant distance on the circuit boards. Power and high voltage are delivered by discrete wires (Type 1 services ÃćÂĂÂŞ section 8.4.4) terminated in solder holes or pads next to each connector. Signals are routed on broad-side coupled 100 μm wide traces with 75 μm core thickness for impedance control. Nominal impedance is 70 Ω. The rigid boards have three metal layers, with the buried layer 75 μm under the top layer, and a 1.6 mm total thickness.

5.4 Type 1 Electrical Service Assemblies

The Type 1 electrical service assemblies include all low-voltage power lines for the pixel modules and optical readout, high-voltage lines for the pixel modules, lines for temperature monitoring of the pixel modules and opto-boards and lines for environmental(temperature and humidity) monitoring within the Pixel Support Tube.

At one end, twisted pair electrical lines are soldered to the PP0 printed circuit board or soldered or crimped to connectors for environmental sensors. The twisted pair wires are soldered at the PP1 end to thin, printed circuit boards. The area available at the end of the Pixel Support Tube is insufficient to allow for penetration of the twisted pair wires. Thus there is a transition made in this region from twisted pair to thin printed circuit boards. These PP1 printed circuit boards are laminated together (section 8.4.7) thereby substantially reducing the cross-sectional area for the services in the very crowded region at the end of the Pixel Support Tube. Short twist-pair wires are soldered to the other end of each printed circuit board and connected to a multi-pin connector(***Ref. LEMO...***).

The components of the Type I assemblies, internal twisted-pair wires of different gauges, PP1 printed circuit boards, external twisted-pair wires and multi-pin connectors were assembled in

pairs(Ref LEMO USA) to form single 5-m long assemblies of three types: low-voltage power, high-voltage and optical power/environmental. The wire types and gauges for the different assemblies are summarized in Table 8.4.1. Copper-clad aluminum magnet wire is a standard industrial product containing 10

	Number of Twisted Pairs	Wire Type	Conductor Diameter	Insulation
Low Voltage Power			(μm)	
Internal	14	Solid copper-clad aluminum	813	Polyurethane
	14	Solid copper-clad aluminum	643	Polyurethane
	28	Solid copper-clad aluminum	404	Polyurethane
External	28	Stranded-tin-plated copper	7x150	Polyimide
	28	Stranded-tin-plated copper	7x120	Polyimide
Optical control and Environmental				
Internal	44	Solid copper	127	Polyurethane
External	44	Stranded-tin-plated copper	7x120	Polyimide
High Voltage Internal	26	Solid copper	127	Polyimide
External	26	Stranded-tin-plated copper	7x120	Polyimide

Table 9. Components of the Type I electrical services assemblies described in the text.

All soldering was done by hand. The connectivity and resistance of each circuit was measured using commercially available, computer-controlled cable checkers (****Ref...****) during the assembly process and after completion of the assemblies. Resistances were compared to nominal values and deviations outside acceptance windows triggered repair procedures. All completed assemblies were required to have 100% connectivity and to have acceptable resistance values. There are about 320,000 solder joints in all assemblies.

The completed assemblies were cut in the middle and each twisted pair soldered to the appropriate location on the PP0 printed-circuit board assemblies or crimped/soldered to small connectors for the environmental sensors. Extensive quality control procedures were used to verify the correct connectivity and again to measure the resistance of each circuit after making the PP0 printed circuit board connection. Repair procedures were completed (on approximately 0.1% of the circuits) and 100% connectivity and acceptable resistance were required for the Type I PP0 assemblies.

5.5 Optical Components

Some elements of the optical system are described here and the remainder in section 8.5. The optical boards containing electronics, VCSELs and PIN diodes have already been described in Section 4.

Fiber ribbons are connected to the opto-boards on one end and to a custom connector at PP1. Each of the opto-boards is connected at PP0 by a bare ferrule of an MT8-connector without a connector housing to an 8-way radiation hard SIMM optical fibre ribbon. Two 8-way ribbons coming from PP0 go into an MF16 (MF-A1/MT16) connector which fits into the custom made PP1

connector(described below). There are 494 “long"(251.0 cm) and 246 “short" (226.0 cm) bare (no protective coating) ribbons. The eight PP1 connectors (1 per quadrant of side A and C) incorporate the MF16 connectors of the 320 double ribbons. The machined, aluminum PP1-connector (Ref manufacturer) is shown in Figure 8.4.8.

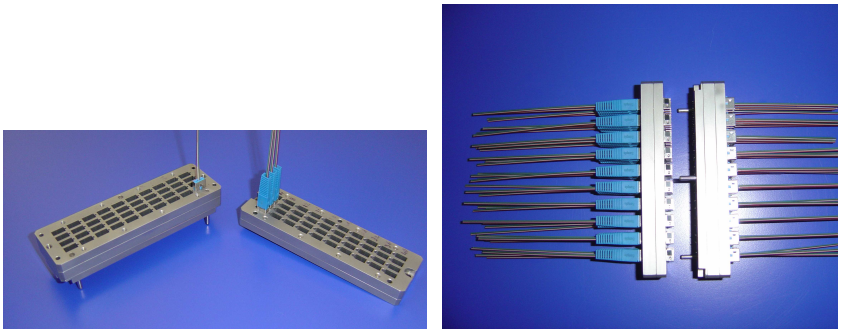

Figure 27. Custom connector at PP1 for connection of the optical ribbons. There is one such connector per quadrant at PP1.

Three steps were taken in the testing of the optical ribbons during the assembly of the Service Quarter Panels. **Pre-assembly**

Each optical fibre was subject to a visual inspection to make sure it was not damaged during handling or labelling. Then, after a calibration procedure, they were tested to ensure that the attenuation was within expectation ($< 20\%$ excluding losses from additional test fibres). Any ribbon failing this test, was retested at the end of our test cycle to verify whether it needed to go back to the manufacturer or if the results were biased due to operator error or some dust on the connector-mating surface.

Post Installation (no optoboard connected)

The same pre-installation test was run after the fibres were installed in the Service Quarter Panels. This test ensured that there were no breaks during the installation.

Optoboard connected

Here the complete opto-link (including the fibers) was tested (see Section 4 for more details and definitions). After the opto-boards were installed, the best VISET and DAC settings for DRX were obtained. Then, a pseudo-random signal was sent from the BOC in a test configuration. This signal was fed back from the PP0 connectors to the opto-boards and was compared with the original signal. If there were no changed bits during this test, it meant that both opto-board and the connecting fibers worked as expected. If a link failed this test, both opto-board and the fibres were retested, and in some cases replaced.

5.6 Cooling System Components

A schematic view of the cooling system components within the region of the Pixel Support Tube is shown in Figure 8.4.9. We provide a brief description of these components here. The overall ATLAS evaporative cooling system is described in Ref. ***???***.

The C_3F_8 fluid enters the pixel volume at PP1 at a temperature of $+20°C - 35°C$ and a pressure of 11-15 bar absolute. The fluid passes through the inlet side of a heat exchanger and is pre-cooled

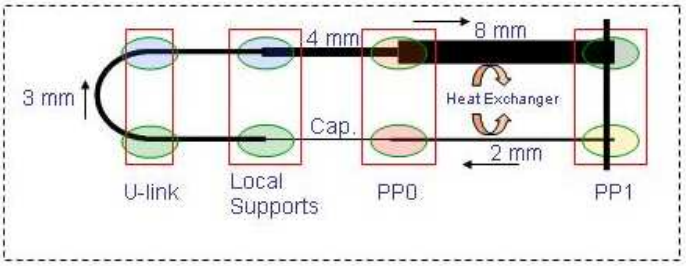

Figure 28. A schematic representation of the components of the pixel evaporative cooling system within the region of the Pixel Support Tube (indicated by the dashed line). The approximate inner diameters of the various tubes are shown apart from the capillary tubing (Cap. In the Figure).

before reaching a capillary tube? at PP0. The length and diameter of the capillary tube is selected to provide a substantial pressure drop, typically up to about 10-12 bar absolute for most circuits. The pressure in the local support or other circuit (for the opto-boards) is controlled by an external regulator (back pressure regulator) in the exhaust line well outside the pixel detector volume(Ref. evap cooling paper again). The fluid enters the local support and evaporation occurs from the heat of the pixel detector modules and associated services. The normal evaporation pressure in the barrel and disk regions is nominally less than 3 bar absolute, leading to an evaporation temperature as low as $-25°C$. The opto-board cooling circuits are normally operated at a higher pressure, up to about 5.5 bar absolute. In the barrel region, two local supports staves are connected by a custom-fabricated U-link and similarly in the disk region two sectors are connected by a U-tube. The fluid exits from a local support through custom-bent tubes and then passes to the exhaust side of the heat exchanger, thereby cooling the entering fluid. Custom, low-mass connectors of a single-design concept(but with varying dimensions) are used at each connection within the pixel volume: at PP1 to connect external pipes to the inlet or outlet of the heat exchanger; at PP0 to connect either capillaries or exhausts from the local supports; at the local supports and at U-links (U-shaped pipes) connecting two local supports. We describe briefly each of these components below. A summary of the number of circuits and basic operating parameters is given in Table 8.4.3 and a summary of tubing sizes and types, not including the local supports (already described in previous sections), is given in Table 8.4.4.

	Number of Cooling Circuits	**Nominal Flow Rate (g/s)**
Barrel Region	56	4.2-4.6
Disk Regions	24	2.3
Optical Readout	8	4.3
TOTAL	88	

Table 10. Pixel detector cooling circuits and basic operating parameters.

Heat Exchangers

A schematic view of a heat exchanger is shown in Figure 8.4.10. All heat exchangers are

Item	Material	Number	ID(mm)	OD(mm)
Heat exchanger-inlet	Aluminum	88	2.07	2.78
Heat exchanger-outlet Type 0	Aluminum	88	4.05	4.76
Heat exchanger-outlet Type 1	Aluminum	88	8.92	8.73
Barrel capillary	Copper-Nickel	56	0.8	0.98
Disk capillary	Copper-Nickel	32	0.55	0.98
Opto capillary	Copper-Nickel	8	0.8	0.98
Barrel exhaust	Aluminum	56	4	4.71
Disk exhaust	Aluminum	24	4.05	4.76

Table 11. Tube types and sizes for components of the internal cooling circuits.

functionally identical and consist of two aluminum pipes bonded along their length with a thermally conducting epoxy (Ref goes here) The length over which the tubes are glued is 1.92-2.02m.

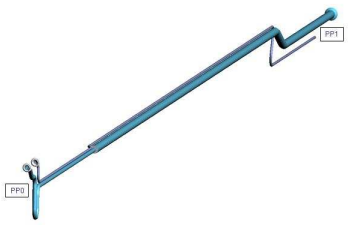

Figure 29. Schematic view of a typical heat exchanger as described in the text.

The inlet-side of the heat exchanger is a single tube running from the PP1 region to the PP0 region. The exhaust side of the heat exchanger consists of a larger-diameter tube (Type 1 region in Table 8.4.4) coupled through a welded transition piece to a smaller- diameter tube (Type 0 region in Table 8.4.4). The smaller diameter is required to fit the tube between connectors on the PP0 printed circuit board(see Figure 8.4.7). The tubes were bent at the PP1 end to match the appropriate hole pattern in the PP1 endplates (described in section 8.4.7). The tubes were bent at the PP0 region to match the inlet and exhaust tubing from the active detector region ÃćÂĂÂŞ see Figure 8.4.11. A U-bend was made in each exhaust section to facilitate small motions of the tubes installation of the pixel detector, to allow easier mating of the connectors and to allow for small changes from thermal contraction.

All heat exchanger assemblies were tested. The inlet or exhaust side of the heat exchanger was connected to a helium leak checker on one end and the other end plugged. Leak checks were completed after assembly and after pressure cycling the inlet (outlet) to about 20(16) bar absolute, respectively, 50 times. **Capillary Assemblies**

Capillary assemblies consist of small-diameter, copper-nickel (Cu-Ni) tubing adhesively bonded to fittings (described below) on each end. The Cu-Ni tubing was produced by a custom extrusion (Ref or footnote goes here). The interior dimensions were different for the barrel/optical and disk

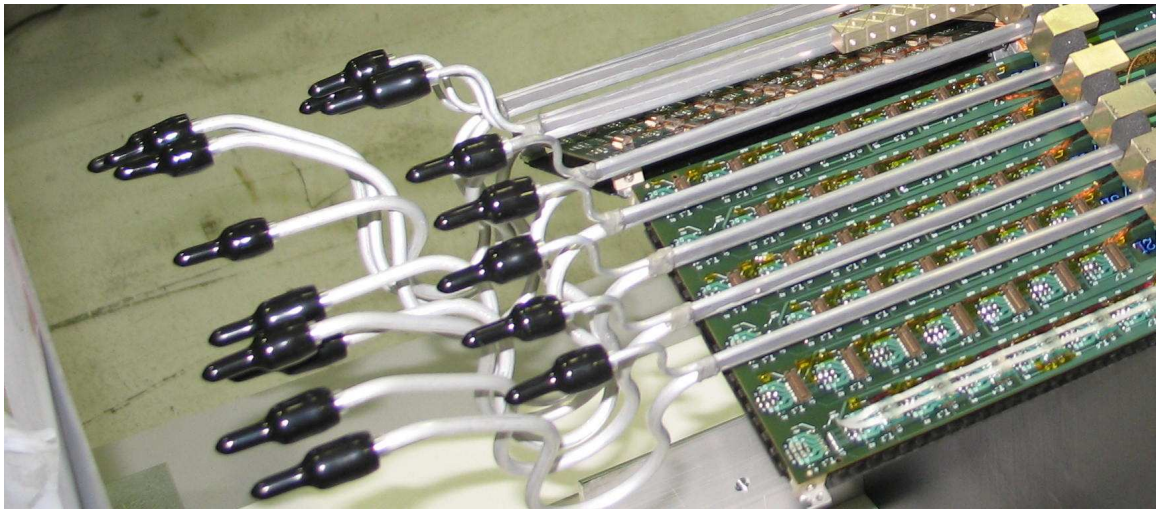

Figure 30. Photographs of heat exchangers at the PP0 end as described in the text. The black objects are temporary protection for the ends of the tubes.

capillaries. The inner and outer diameters are summarized in Table 8.4.6.2. The length of each capillary was adjusted by making a comparison of a precise measurement of the pressure drop of nitrogen gas at a fixed flow rate across each capillary to the same measurement using a reference capillary (separate reference capillary for barrel and disk). Capillaries for barrel Layer 2 were approximately 110 cm long and capillaries for barrel layers 0 and 1 were about 120 cm long. Disk capillaries were also about 120 cm.

The ends of the capillaries were adhesively bonded (footnote Hysol 9394) to aluminum fittings (described in more detailed below). A picture of a capillary bonded to a fitting is shown in Figure 8.4.12a and Figure 8.4.12b.

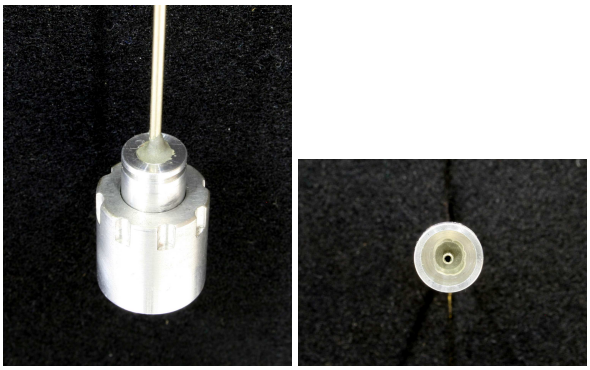

Figure 31. Capillary bonded to aluminum fitting. (a) View from the back of the fitting and (b) view from the front of the fitting.

Each capillary was tested by connection to a helium leak checker after assembly, after thermal cycling 50 times from about $20°C$ to about $-25°C$ and after pressure cycling to 20 bar absolute also 50 times. **U-links and U-tubes**

Connections between two staves in the barrel region and two sectors in the disk region were made by U-links and U-tubes, respectively. A U-link is shown in Figure 8.4.13a. The design of the U-link is driven by tight space constraints at the ends of the staves. The U-link is a machined and bent small aluminum structure made with multiple e-beam and laser welds. A U-tube is a simple round tube bent into a U-shape to which the appropriate fittings are attached by laser welding (see Figure 8.4.13b).

Figure 32. (a) U-link structure used to connect to staves to form a bi-stave unit and (b) U-tube for connecting disk sectors, during assembly of a disk.

Local Support Exhaust Tubes

Local support exhaust tubes are attached at the exhaust-end of a bi-stave or bi-sector cooling circuit to route the fluid to the heat exchangers. The tube diameters are given in Table 8.4.4. The local support exhaust tubes are custom-bent aluminum tubes. In the barrel region, 56 different tube types - each tube was a unique shape - were bent by a commercial three-dimensional bending process (Ref vendor). In the disk region, there were three types of tubes corresponding to the three disk positions and were bent by hand using forms. Custom fittings were attached by laser welding, as described below. **Custom Fittings**

Custom fittings were used throughout the region inside the Pixel Support Tube and at Patch Panel 1 to connect the cooling pipes and capillaries. Custom fittings were chosen to minimize material (radiation lengths) compared to commercially available fittings and to provide functionality (electrical isolation) not found by commercially available fittings.

Tapered, aluminum m:etal-to-metal fittings were used within the pixel detector volume except at the PP1 region. The concept of the tapered fitting is shown in Figure 8.4.14(a). The appropriate aluminum pipe (Table 8.4.4) was welded (Ref EB Industries) to these fittings, as shown in Figure 8.4.14(b). Fittings were also glued to capillaries, as already described above.

This type of fitting was used to for all cooling connections within the Pixel Support Tube except for the end of the heat exchangers at the PP1 region. An electrical break at PP1 for both inlet and exhaust lines of the heat exchanger was implemented as shown in Figure 8.4.15 for an inlet line. The glass-filled PEEK ferrule is a glued assembly that also contains a filter screen with

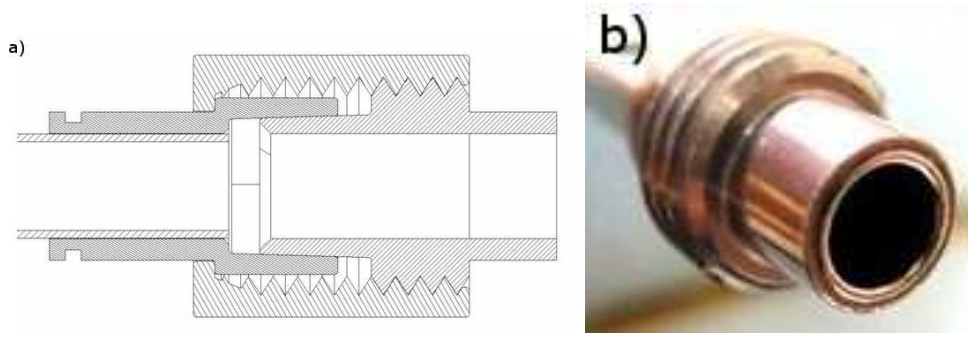

Figure 33. (a) Concept for tapered aluminum, metal-to-metal fitting; (b) fitting with welded aluminum pipe.

pore diameter of 380 microns. The inlet or outlet tubing is flared and makes contact with the ferrule held by a nut and threads to provide a leak tight seal.

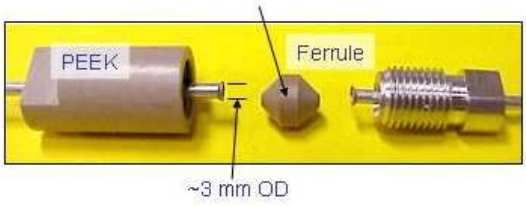

Figure 34. Example of an inlet fitting at PP1 that provides also electrical isolation between the two sides of the circuit.***Will improve***

5.7 Service Quarter Panels

The electrical, optical and cooling components described above were integrated into eight Service Quarter Panels (SQP), four on each side of the detector. We first provide a brief overview of the SQP structure and then describe the assembly and testing of an SQP, including a few components not already described above.

An overview of an SQP is illustrated in Figure 8.4.16. The Type 1 electrical services are not shown in this illustration.

An SQP consists of the following principal substructures (described in more detail below):

- A “backbone" structure that supports the heat exchangers, a PP1 aluminum endplate and structures for optical ribbon support and routing;
- Two inner and two outer service panels that each contain the Type 1 electrical services attached to the PP0 printed circuit boards (as described previously); and
- A cooling circuit for the opto-boards finally mounted on the PP0 printed circuit boards.

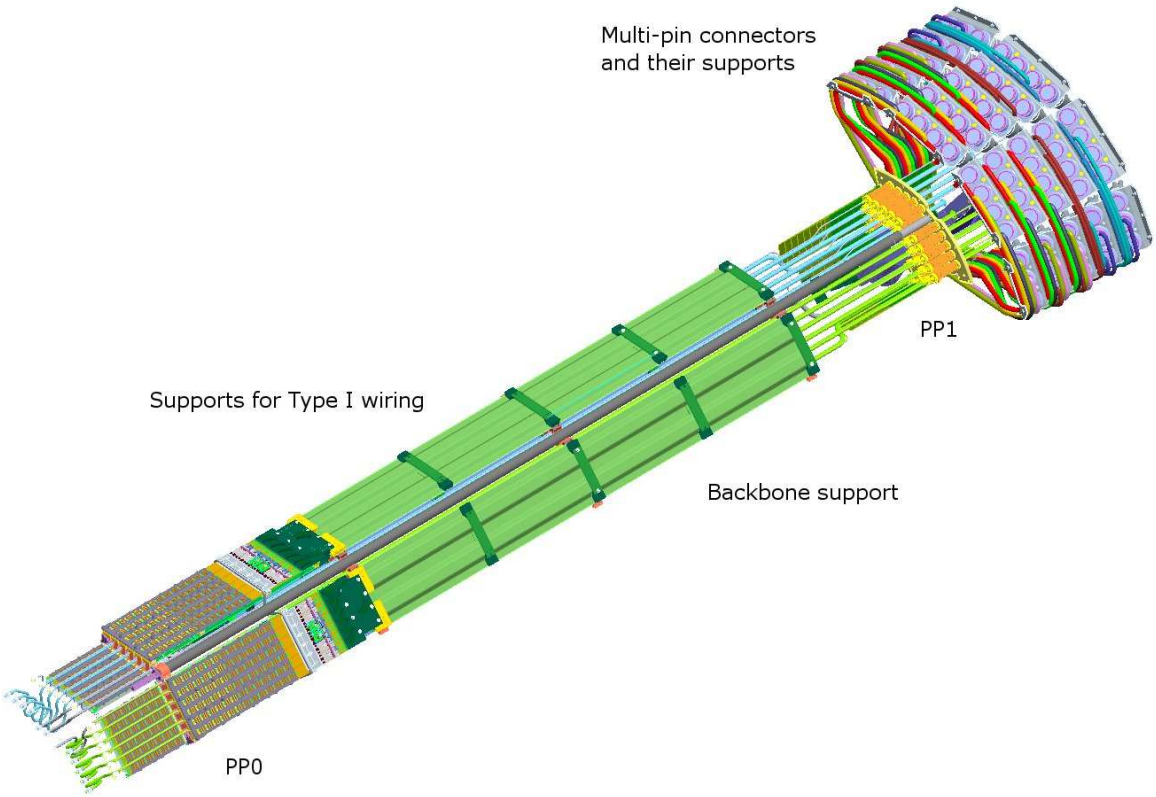

Figure 35. Illustration of a SQP. The internal Type 1 electrical services are not shown for clarity.****Annotation needs to be fixed****

Photographs of the backbone structure are shown in Figure 8.4.17a (overview) and Figure 8.4.17b (detail PP1 region). This structure consists of a carbon-fiber tube (custom manufactured) to which support arms are attached. The support arms are either machined aluminum pieces(at the PP0 end only) or plastic pieces fabricated by a stereo lithography process to provide a complex shape(Reference here). Additional plastic pieces (also manufactured by stereo lithography) for routing fibre ribbons are adhesively bonded to the carbon fiber tube as shown in Figure 8.4.17b.

The backbone is attached to a machined aluminum plate at the PP1 end, the PP1 quarter plate that has penetrations for the heat exchanger tubes, the Type 1 electrical services (laminated printed circuit boards), the connection of nitrogen gas to provide a dry atmosphere inside the Pixel Support Tube and a penetration for the routing of optical fibers to the PP1 optical connector plate. An illustration of the PP1 region is shown in Figure 8.4.18.

The heat exchangers are placed into the support arms of the backbone structure and the inlet and exhaust pipes penetrate through the PP1 quarter plate as shown in Figure 8.4.18. Bellows-assemblies are attached to each heat exchanger and to the PP1 quarter plates. These assemblies provide a gas seal by using a thin-wall, but tight-fitting PEEK sleeve around each heat exchanger

Figure 36. (a) Overview of Service Quarter Panel backbone and (b) expanded view at the PP1 region, as described in the text.

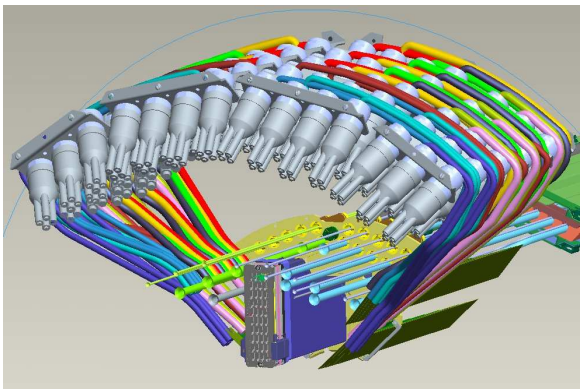

Figure 37. Illustration of the PP1 region with the components described in the text.

tube and threaded PEEK insert that connects to the PP1 quarter plate. The copper bellows, glued to the PEEK parts, are necessary to allow for contraction of the heat exchangers during cold operation by 2-3 mm. The region of the bellows is shown in Figure 8.4.19.

A service panel assembly consists of a PP0 printed circuit board unit connected to a corrugated carbon-fiber support that holds and guides the Type-1 electrical services that are soldered to the PP0 unit. Plastic structures (manufactured by stereo lithography) and mounting tabs are mounted to a service panel. An inner service panel mounts to the backbone structure on the side closer to the beamline of ATLAS (inside). An outer service panel mounts to the outer side of the backbone structure.

The services panels are connected with small aluminum screws to the support arms of the backbone structure. The laminated printed circuit boards from each Type-1 electrical services bundle are captured by an aluminum flange that bolts to the PP1 quarter plate. A photograph of the region near the PP1 quarter plate is shown in Figure 8.4.20. The complexity of the connections and the tight clearances are evident from this photograph.

Opto-boards are mounted to the PP0 printed circuit boards (by their respective connectors).

Figure 38. Heat exchangers loaded into a backbone in the region of the PP1 quarter plate showing the bellows-assembly seal described in the text.

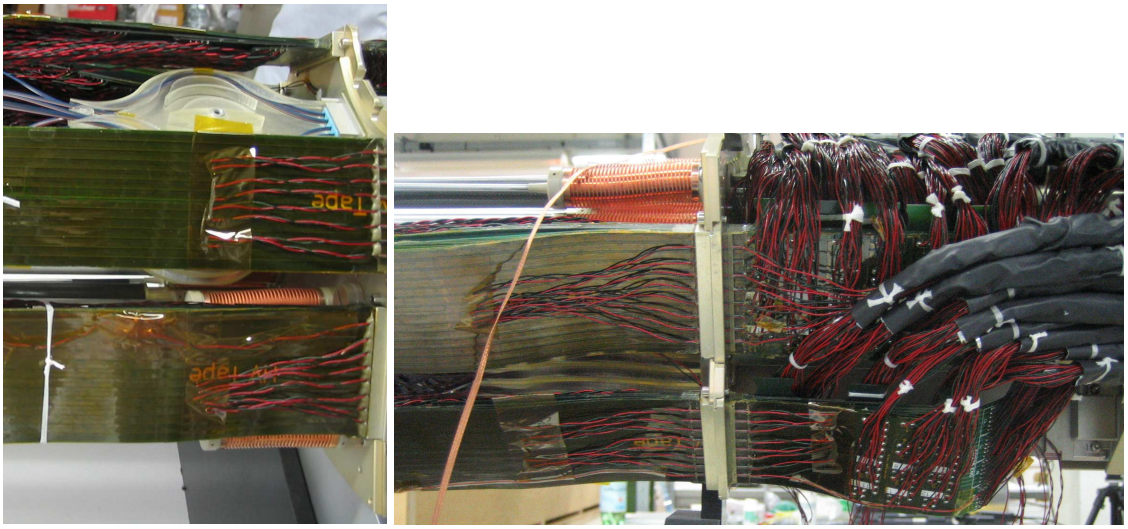

Figure 39. Region near a PP1 quarter plate after the attachment of inner and outer service panels.

The optical fiber ribbons are attached to the opto-boards and routed along a service panel to a plastic structure attached to the PP1 quarter plate that captures the ribbon but that can take up slack in the ribbon needed for attachment to the PP1 optical connector. One of these plastic structures may be seen in Figure 8.4.20 (left portion of the figure), and these were also made by stereo lithography. The fibers are routed through the PP1 quarter plate and into a box structure (not yet in place in Figure 8.4.20, left portion) to which the PP1 connector plate is attached. The box structure is needed to position the connector plate away form the PP1 endplate to allow access.

Temperature control of the opto-boards is accomplished by a cooling circuit that routes coolant to aluminum structures and fingers brought into contact with the opto-boards through a thermal-grease interface(****Reference goes here****). A photograph of the thermal fingers and structures in contact with the opto-boards are shown in Figure 8.4.21.

During the initial testing of opto-boards on a prototype Service Quarter Panel, it was realized

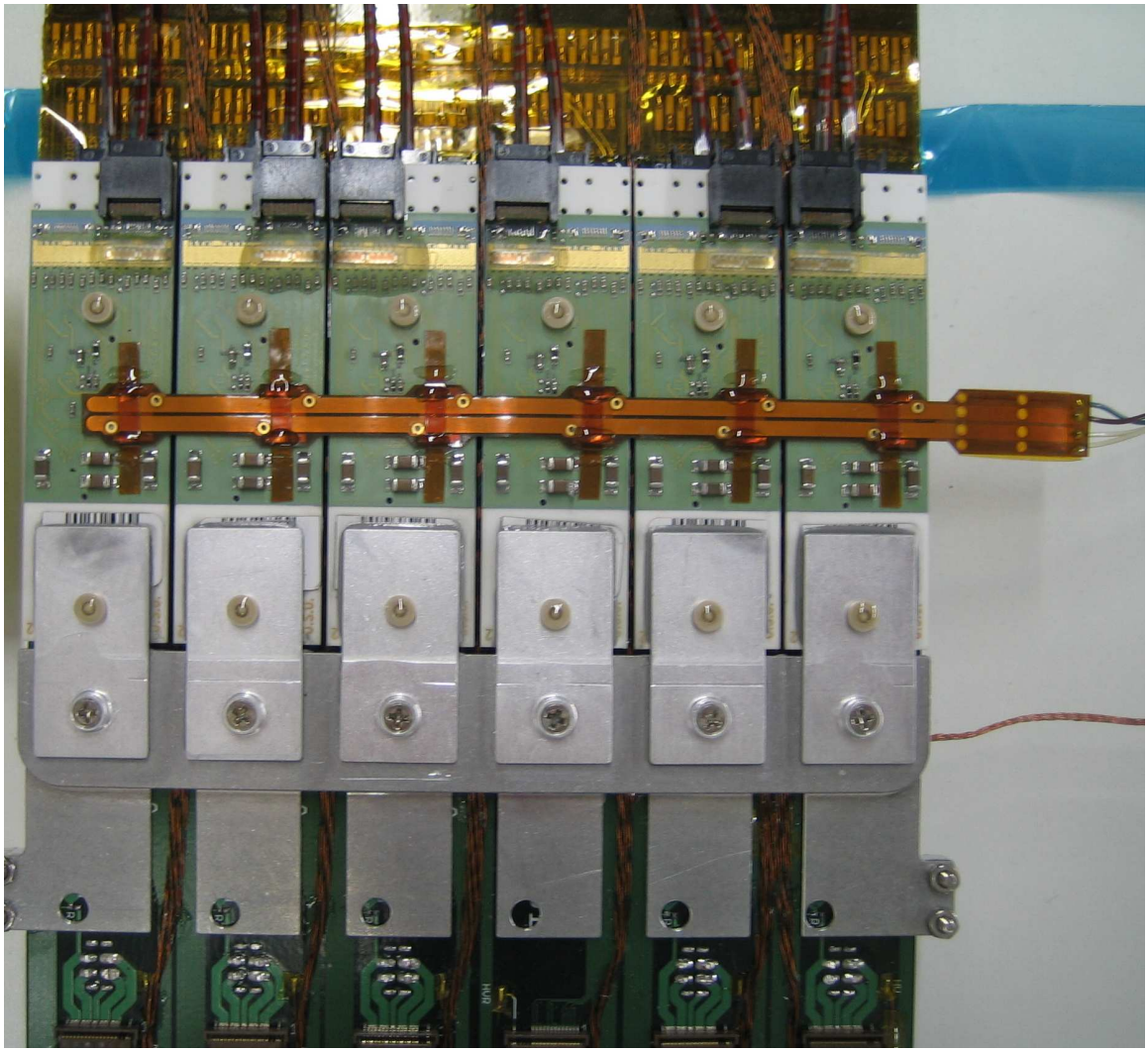

Figure 40. Photograph of the cooling connection made to the opto-boards, as described in the text.

that additional thermal control of the opto-board temperature was required, in particular to prevent the opto-board temperature from being too cold. The additional thermal control was instituted largely after the fabrication of the service panels had been completed. The additional elements consist of copper-on-kapton heaters attached (glued as seen at the top in Figure 8.4.21) to the opto-boards and a thermal “blanket" shaped from a kapton-copper laminate that was placed over the opto-boards such that self-heating would also increase their temperature. These heaters were connected to small, multi-wire cables passing through a spare hole in the PP1 quarter plate and connected externally to controllable power supplies to regulate the temperature.

We very briefly describe the assembly and testing of the Service Quarter Panels here. All of the mechanical, cooling and electrical services components of the Service Quarter Panels were made or integrated at a single production site in the United States. The assembly of service panels and integration of heat exchangers with the backbone supports and PP1 quarter plates occurred at

this site. Extensive quality control procedures were implemented for the Type 1 electrical services to verify connectivity and measure resistances at each major step of the assembly of the service panels. Outer service panels were attached to the loaded backbone structure for each of the eight SQP. These substructures were shipped from the United States to CERN. The inner service panels were shipped separately.[8]

The final integration of the SQPs occurred at CERN. Opto-boards were attached to the service panels and fibre ribbons connected. The pixel detector has 272 opto-boards with 316 VCSEL and 272 PiN packages on-detector. Extensive qualification testing was done for the optical system. Three steps were taken in the testing of the optical ribbons. Each optical fibre was subject to a visual inspection to make sure it was not damaged during handling/labeling. Then, after a calibration procedure, they were tested to ensure that the attenuation was within expectation (less than 20% excluding losses from additional test fibres). The same test was run after the fibres were installed in the SQPs. This test ensured that there were no breaks during the installation. Once the opto-board was attached, the complete optolink (including the fibers) was tested. The best VISET and DAC settings for DRX were obtained. A pseudo-random signal was sent from the BOC card at the test setup. This signal was returned from the PP0 connectors to the opto-boards and compared with the original signal at the test setup to find the number of bits that changed. If a link failed this test, both opto-board and the fibers were retested separately. Parts that failed were replaced such that the final yield for a SQP was 100% at this stage of assembly.

Inner service panels were attached at CERN. This included also complex routing of temperature and environmental connections.

The final step in the completion of the Service Quarter Panels was to prepare the external Type 1 services and heat exchangers to allow for insertion of the assembled pixel package into the Pixel Support Tube (see section 8.8 and 8.9). The clearance between the inner diameter of the Pixel Support Tube and the outer radius of the quarter plate was only a few millimeters. Thus it was required to bend and compact temporarily the external Type 1 electrical services to allow them (on one side) to pass through Pixel Support Tube. In order to do this, a protective aluminum structure was made to fit over the heat exchanger tubes exiting from the PP1 quarter plate.

The external Type 1 electrical services were bent and compressed and held to the protective structure as shown in Figure 8.4.22. Temporary extensions of the heat exchanger pipes were added before this stage such that vacuum leak checking could be done during the final integration of the SQP with the cooling circuits of the pixel detector (see section 8.8). These extensions are partially visible in Figure 8.4.22.

A completed SQP was transported to the integration site of the pixel detector package, described in Section 8.8.

6. External Services

External services include electrical cables, optical fibers and cooling pipes that connect to the pixel detector at the PP1 region ÃćÂĂÂŞ see Figure 8.5.1 for reference to cable types and patch panel logical locations.

[8] One SQP was shipped with both inner and outer service panels attached to the integrated backbone structure.

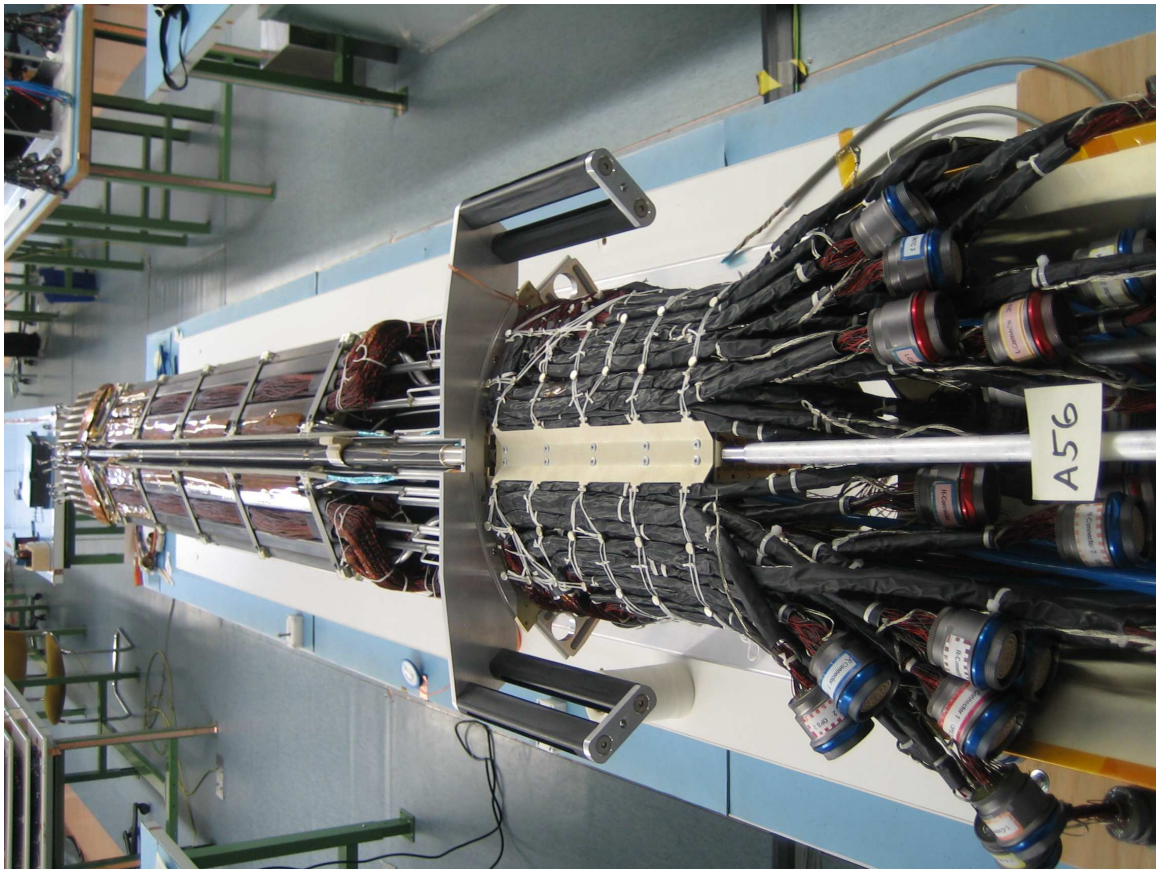

Figure 41. Photograph of the external Type 1 electrical services compacted as described in the text.

Patch panels and active elementsÃć voltage regulatorsÃć are also part of the external pixel services. An overview of the Data Control System and its components has already been given in Section 4.6. We describe here additional elements of the external services and related systems.

All the services have to be disconnected at PP1 to allow for removal/installation of the pixel system. While at PP0 and PP1 all the cables and cooling connections are located close together in the same area, cables, fibres and cooling tubes at the other patch panels are placed in different locations because they are subject to different requirements. In general the component used between PP1 and PP2 have to be radiation resistant (up to $5x10^5$ Gy), while the more external components use standard material.

The PP2 locations for the cables are placed in specifically designed platforms after the first layer of the muon spectrometer system. The PP3 locations are outside the ATLAS active detector volume. The PP4 locations are in the counting rooms, close to the power supply units.

Each PP2 platform hosts a different combination of active regulation stations (described in 8.5.4) and passive patch panels for the temperature and environmental monitoring signals. Space constraints, the high number of connections per platform and the position inside the toroidal magnetic field has required a careful design to allow maintenance during operation.

PP3 is mainly the place where the front end components of the DCS are located:BBIM, BBM

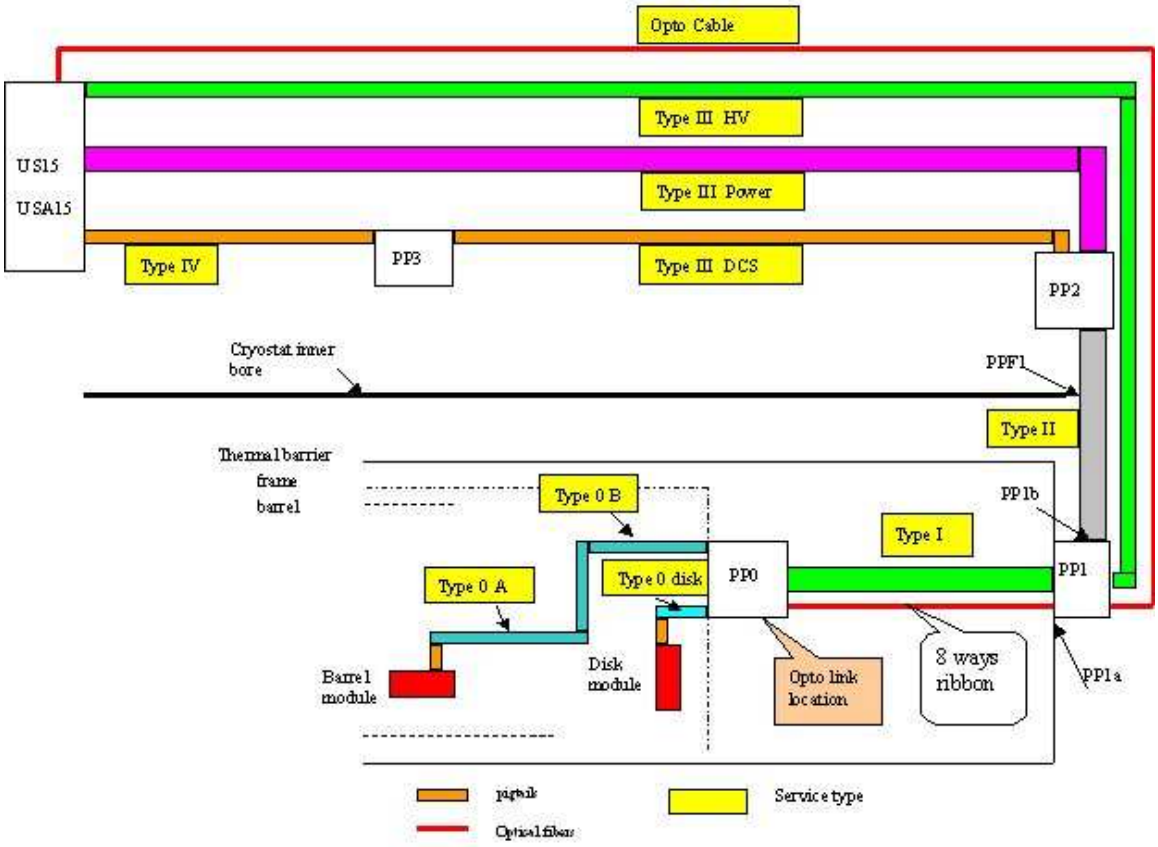

Figure 42. Overview of the pixel internal and external services and patch panels.

and optical services. All the temperature and environmental monitoring signals and opto services go through PP3. For the opto-services cables, PP3 is only a break point, while for all the other signals monitoring function also create the logical signals for the interlock system.

6.1 Cooling Pipes

Connections to the ATLAS evaporative cooling system are made at PP1. A photograph of the PP1 region, before connections were made to the external services, is shown in Figure 8.5.2. Custom bent aluminum exhaust and inlet pipes are used to connect the corresponding pipes from the heat exchangers (described in 8.4.6) to external stainless steel blocks located about 40 cm from the beamline to which copper pipes have been brazed. Photographs of these custom pipes are shown in Figure 8.5.3a and Figure 8.5.3b. There are 53 different geometries made by custom pipe bending. A fitting is attached by laser welding to one end and this end bolts into the stainless steel block. The remainder of the evaporative cooling system is described in Ref.******

6.2 Optical Fibers

The internal optical fiber ribbons and the connector at PP1 have been described in the previous section. The connection outside the pixel detector between PP1 and USA15 is done by optical

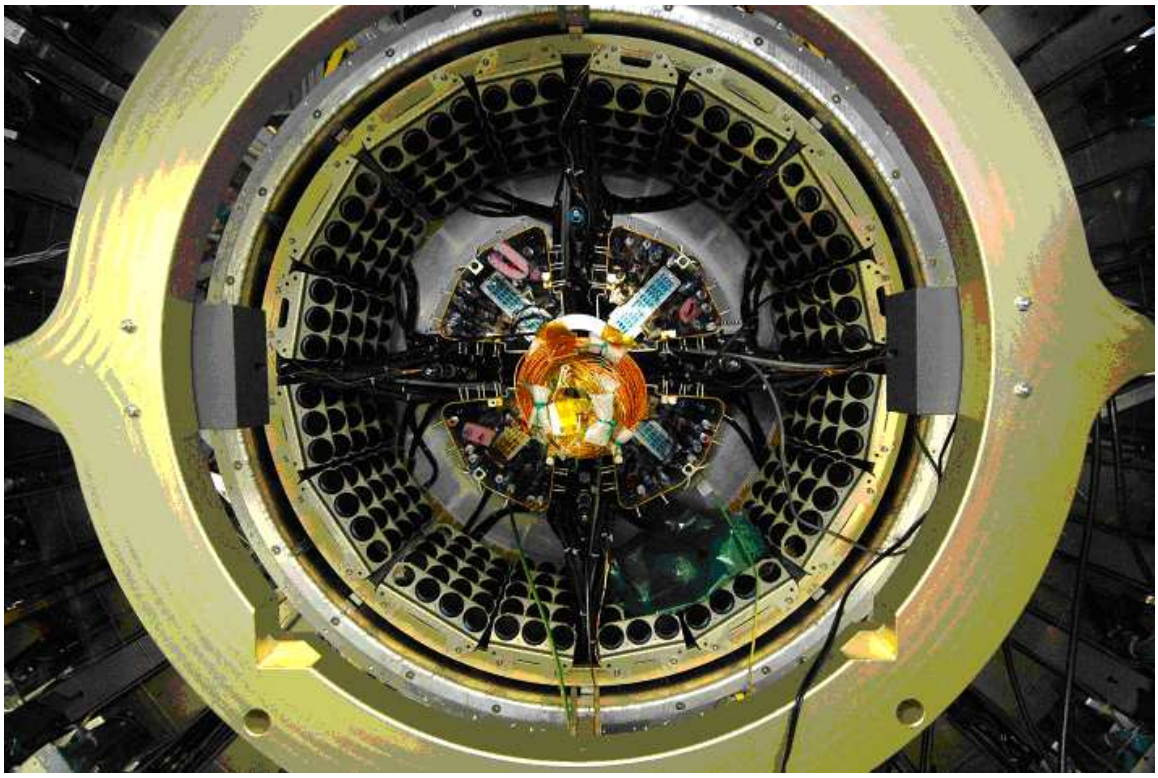

Figure 43. Photograph of the PP1 region at the end of the Pixel Support Tube before connection of external services.

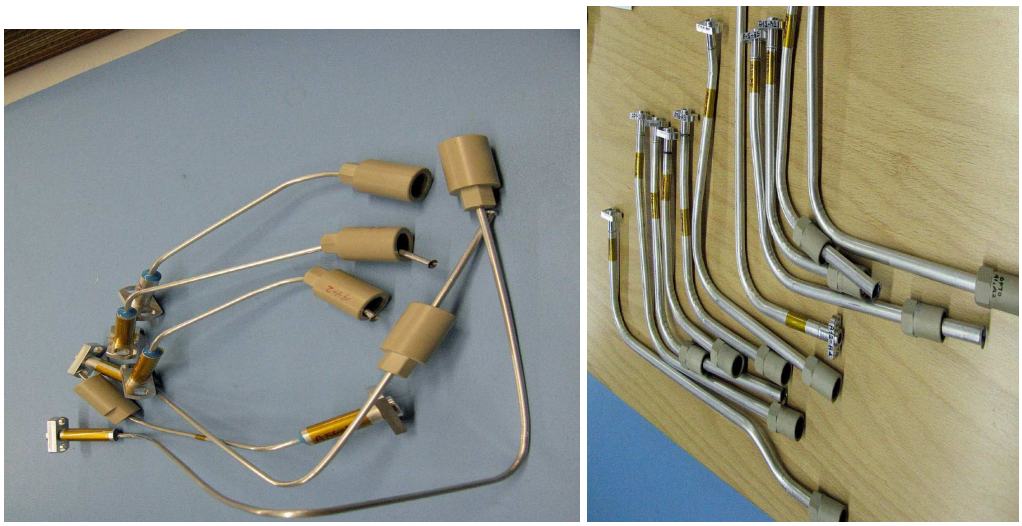

Figure 44. Photograph of the custom pipes connectng PP1 to the ATLAS evaporative cooling system.

unitube fiber cables that contain eight 8-way ribbons each. Though there are eight single fibers in a ribbon, only 6 or 7 fibers are actually used for transmitting data from the modules or receiving

TTC information for the modules.

The total number of single fibers for the pixel detector is 3774. The inside of the ATLAS detector is a zone of high radiation limiting the lifetime and the light transmission of optical fibers. Outside the ATLAS detector the radiation levels will be considerably lower than the ones inside. Therefore radiation hard SIMM50[9] multi-mode fibers are used inside the ATLAS detector (the fiber ribbons described previously) and radiation tolerant GRIN50[10] fibers for timing and GRIN62.5 fibers for data transfer outside of the detector.

Eighty optical unitube fiber cables transfer the data and timing information between PP1 and the counting room in USA15. The unitube cable has a protective sheath of halogen free flame retardant polyethylene (HFFR-PE). In addition, there are two spare fiber cables per side. The 84 fibre cables consist each of 8 about 8.1 m long radiation hard SIMM50 ribbons which are fusion-spliced to 8 about 71.1 m long radiation tolerant GRIN50/62.5 ribbons. The total length of the stainless steel tube that protects the spliced joint is about 60 cm and over this length the cable diameter grows from 0.95 cm to 1.4 cm. This technique of splicing avoids having any additional patch panel and there is the advantage that splicing is cheaper and more reliable than connectors.

All internal ribbons and all 84 optical fiber cables were tested at the factory in a configuration similar to the installation configuration in the ATLAS detector. Light was injected at the PP0 end of the ribbon and detected at the USA15 end of the fiber cable. This method measures the total light loss. The attenuation of the light signal was smaller than 2.5 dB for the data transfer lines, and smaller than 3.5 dB for the TTC lines.

After installation of the optical fiber cables in the ATLAS cavern, all 84 cables with their 672 ribbons were tested with an optical time domain reflectometer (OTDR) in order to guarantee that no fibers were damaged during cable instalation and fixation in the electronics racks.

6.3 Electrical Cables and Patch Panels

The functional location of the Patch Panels(PP2, PP3, etc) is defined in Figure 8.5.1. We summarize here the principal parameters of the electrical cables (see Table 8.5.1). **Type II Low-Voltage Cables**

A low-voltage Type II cable is a bundle of three sub-cables. Two cables (VDD,VDDA) have seven (***check number***) twisted conductors (2xAWG20, 1 xAWG22, 1 AWG28). The third cable, VVDC, has one twisted quad-set of conductors of (3 xAWG22, 1 AWG28)(***is this sentence complete***?). These sub-cables are insulated with SILTEM(Footnote SILTEM is a flexile siloxane-polyetherimide polymer, non-halogenated, that is used for cable coating and has been qualified as radiation resistant at a level higher than the $5x10^5$ Gy) and electrically shielded. The bundle is DC-grounded at PP1 and AC-grounded at PP2. The cable bundle is terminated at PP1 with a 64-pin connector[11] and at PP2 with a 66-pin connector[12] A total 276 are installed. **Type III Low-voltage Cables**

Low-voltage Type III cables are individual cables with standard insulation. A VDD (VDDA) cable has seven twisted pairs of AWG16 (AWG14) wire, while a VVDC cable has one twisted pair

[9] Step Index Multimode fibre from Fujikura***need full name here***

[10] GRIN-Graded Index fibre from Draka ***need full name here***

[11] LEMO Series 5F (FGW.5F.364.XLC)

[12] Positronics GMCT66M00P0Z0.

Cable Type	Function	Wire Size/Gauge	Wire	Total Number	Insulation Type
Low voltage Type II				276	
	VDD	2 x AWG20 1 x AWG22 1 x AWG28	7 twisted quad		SILTEM
	VDDA	2 x AWG20 1 x AWG22 1 x AWG28	7 twisted quad		SILTEM
	VVDC	2 x AWG20	7 twisted quad		SILTEM
Low voltage Type III				276	
	VDD VDDA VVDC	AWG16 AWG14 AWG18	7 twisted pair 7 twisted pair		
High voltage				336	
	High voltage	AWG26	4 x 7 twisted pair		SILTEM

Table 12. Characteristics of low-voltage and high-voltage cables connecting the pixel detector at PP1 to external power supplies, voltage regulators and monitoring stations.

of AWG18 wire. A VDD or VDDA cable is terminated at both ends with a 34-pin connector[13]. VVDC cables are terminated at both ends on a 9-pin Sub-D connector. **High Voltage Cables**

The high voltage cables run from PP1 to PP4. A HV cable is also a bundle of four ssub-cables. Each sub-cable is made of seven twisted pairs of AWG26 conductors, SILTEM insulated and rated for use at 700V. The high voltage cable bundle is terminated at PP1 with a 64 pin connector[14] and at PP4 with a 22 pin connector[15]. In total, 336 cables are installed. **Patch Panel 2**

The voltage regulation system at PP2 is described below in 8.5.4. *****Other functions briefly here***** **Patch Panel 3 Patch Panel 4**

The connection between low-voltage and high-voltage cables and their respective power supplies is made at Patch Panel 4(PP4). Additional monitoring hardware is also provided at PP4. Connectivity and current monitoring between the low voltage power supplies (VDD and VDDA for each module) and the local regulators at PP2 is implemented. In order to conserve resources, one low voltage supply channel supplies 6 or 7 circuits, corresponding to a half stave or a sector. Ground is common within a group of 6 or 7 circuits but isolated between them. A current measurement is made through a low value, high precision resistor in each of the 6 or 7 circuits. The measurement is then digitized and read out over an Embedded Local Monitoring Board (ELMB) via a CAN bus. The measurements are monitored through the pixel DCS software.

High voltage monitoring functions in a similar manner but at higher voltage and lower current.

[13]Positronic GMCT34M0TLR00

[14]LEMO Series 5F (FGW.5F.364.XLC)

[15]LEMO/REDEL Rectangular High Voltage Connector standard at CERN (SCEM 09.41.34.110.8), 22 pins

Monitoring boards housed in 16 crates at PP4 will monitor up to 117 detector module currents per crate, in the range 0.4 to 4 mA. In addition, the hardware allows the connectivity to change from 6 or 7 circuits per supply channel (current configuration) to only 1 or 3 circuits per supply channel (future configuration), once radiation damage of the pixel sensors causes the high voltage current requirements to exceed the capacity of a single power supply channel. The change can be accomplished by removal of circuit jumpers on VME-form-factor cards at PP4 at the appropriate time. Grounding is common within pairs of circuits and isolated between pairs. Individual circuit current measurement capability, corresponding to a single module, is included in the design and a bad circuit can be disconnected. The measurement is digitized and read out over an ELMB via CAN bus and monitored through the pixel DCS software.

6.4 PP2 Voltage Regulators

The low voltages necessary for the pixel integrated circuits and the inherent resistance of the power supply cables, require voltage regulation to be implemented as close as possible to the pixel detector. Voltage-regulation is provided by custom-designed and custom-built, remotely-programmable regulator stations located at PP2(Refs go here). These stations provide individual power outputs with low ripple and protect the integrated circuit electronics against transients up to 4 volts, the nominal maximum rating of the 0.25 micron integrated circuit electronics. One regulation station powers up to 84 detector modules and also provides power to the opto-boards.

A regulation station consists of 12 printed circuit boards(Regulator Boards) and a Controller Board housed in a custom crate. The unregulated input voltages enter the crate via an input board and are distributed to the Regulator Boards by a custom backplane. The regulated voltages are in-turn provided under computer control by the Regulator Boards and distributed via the backplane to the Type II cables and thereby to the pixel front-end electronics.

A Regulator Board is built on a highly dissipative substrate (approx 20W/board). Each board provides 15 independent voltage channels, 14 for the pixel module electronics and one redundant line for the opto-board. Each board houses 16 rad-hard voltage regulators(Footnote manufactured by ST Microelectronics - LHC4913 positive voltage regulators). Output voltages are programmable in the range 1.4-2.6V, at the load, with a 10mV regulation step. The board has the capability to digitally adjust the output voltage and to monitor voltages and currents of each output channel as well as the temperature of the board. Current compensation is implemented for each voltage and the maximum current per channel is 3A for the module channels and 1A for the opto-board channel.

A Controller Board supervises all operations and communicates with the Regulator Boards and with the pixel data control system. The implementation of the Controller Board is based on an FPGA[16]. The FPGA can be reprogrammed via the CAN bus to allow for adjustments of the voltages and currents provided to the front end electronics during the lifetime of the experiment.

The regulation station will operate in a moderate radiation environment and is required to operate with no degradation up to a total dose of about 140 Gy and a maximum neutron fluence of about $1.3x10^{12}$ MeV n_{eq}/cm^2. The location of the regulation station (PP2) allows a limited possibility of access for repairs. Prototypes of the regulator and controller boards have been extensively tested under radiation. The tests have shown that the performance of the boards is substantially

[16] ACTEL PRO ASIC PLUS APA075

unchanged after radiation. These results have been achieved by proper selection of the components and design.

The mechanical structure of the regulation station is completely enclosed in mechanical panels to ensure proper electrical shielding. The boards are cooled with a dedicated C_6F_{14} circuit similar to that used for other elements of the ATLAS inner detector. The 28 regulation stations are distributed in 12 different locations near the first layer of muon chambers in the ATLAS detectors, and are mounted in groups of two or three crates.

6.5 Electrical Services Testing

Testing of the electrical services took place during various stages of the installation and during a final test of the full chain, from the counting room at PP4 to PP1 and back. A hardware and software package was designed for this purpose, to ensure that safe connections could be made at PP1 to the internal pixel services and modules. All elements of the electrical chain were tested, including low voltage power supplies, opto-link power supplies, active low voltage fan-outs at PP4, regulator boards at PP2, high-voltage power supplies, passive HV fan-outs at PP4, as well as the complete interlock system. Service tests included basic continuity checks, PP4/PP1 measurement cross-checks, interlock functionality tests and calibration of the voltage regulators at PP2.

Measurements were made at PP1 using hardware with the GPIB (General Purpose Interface Bus) interface, including a set of digital multimeters, switching matrices and a programmable load generator. This hardware was connected to the PP1-end of each of the Type-II cables. The software was responsible for controlling the DCS (Detector Control System) and GPIB hardware to switch through all channels in a cable, supply the proper termination loads and test all channels. The design of the software simultaneously checked the connectivity mapping of the detector, as used in DCS. The full documentation for the service tests summarized above can be found in ATL-IP-QA-0026. Any services responsible for transferring the data to the external read-out system were tested separately during DAQ sign-off (see Section XX).

7. Integration

In this section we summarize the final integration of the major detector sub-elements: the barrel half-shells, the endcap units and the internal services and related supports. The integration of these elements was carried out in large clean-room area (nominally about class 10,000) that was used to assemble all of the Inner Detector sub-detectors.

The pixel detector with internal services was assembled on an 8 m long, custom-built frame, the Integration and Test Tool (ITT). The ITT was constructed to temporarily support each element with high precision until the fully integrated package provided the final support and to allow rotation about the beam pipe axis to facilitate assembly and testing. The basic sequence of assembly was: barrel region outer layers, beam pipe (with temporary supports), barrel B-layer, endcap units, support units for the beam pipe and internal services and finally the internal services. Testing to verify functionality was done in between major assembly steps. The basic assembly sequence is described below.

Barrel Layer 2 and Layer 1 were in turn constructed by clamping together the respective half-shells pre-loaded with bi-staves (described in section 7.2). These layers were inserted sequentially

into the global support frame mounted on the ITT. The Layer 1 and Layer 2 exhaust pipes and capillaries were added only after both full shells were in the support frame.

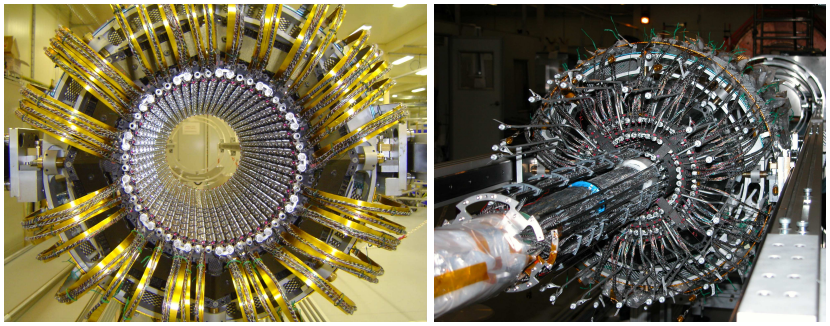

Figure 45. (a) Pixel Layer asembled into global frame and held on the ITT as it appears from looking toward the IP along beam line. (b) The barrel of the Pixel Detector completed.

For the B-layer, exhaust pipes had to be added prior to clamping the shells because of the reduced access to fittings (at the ends of the bi-staves) due to the proximity of the beam pipe. For this reason all the cooling pipes for the B layer are on the C-side, instead of divided between A and C sides as for the outer layers. The B-layer half-shells were clamped together around the beam pipe after the beam pipe was loaded onto the ITT. Figures **??** (a) and (b) show, respectively, Layer 2 in the support frame and the full barrel completed with the beam pipe. Electrical services were temporarily folded back onto the frame.

Both endcap units were fully integrated into their respective support frames at Lawrence Berkeley National Laboratory, including attachment of exhaust pipes and capillaries, prior to transport to CERN. Each endcap was moved into position on the ITT and bolted and pinned for accurate location to the barrel support frame section.

The integration of the Beam Pipe Service Support (BPSS) followed the attachments of the endcaps. The BPSS has the dual function of supporting and adjusting the position of the beam pipe and of supporting the Services Quarter Panels (SQP, described in section 7.4).

The four SQP's per side were mounted sequentially on their respective BPSS, and connections to the detector were made immediately after mounting. SQPs were lifted by a small crane and guided by hand onto the BPSS for final connection. Cooling pipes were connected first and tested. Electrical connectors were then plugged into the SQP, dressed, and tested. Figure **??** shows how the package looked with the first SQP installed. Figure **??** is a view of the detector connector region (PP0) (see section 7.4) after all the services had been connected.

Cooling pipe circuits underwent vacuum leak checks after each fitting connection. Each cooling circuit has a U-link with two fittings connecting two staves or sectors. Each bi-stave or bi-sector is connected to a heat exchanger located in a SQP (see section 7.4). A capillary tube connects the inlet of the bi-stave or bi-sector to inlet side of the heat exchanger. And a custom-bent exhaust tube connects the outlet part of the circuit. A pressurization test at four bar absolute using dry air was carried out for one minute after the capillaries and exhaust pipes had been added and for 24 hours after the full package had been integrated. This test was always followed by a vacuum leak check. This was the highest pressure for which the local supports (sectors and staves) had been qualified.

Figure 46. Pixel package is loaded with the first SQPs on the ITT.

While this pressure should not be reached in the exhaust circuits during normal operation, all inlet circuits must operate at 16 bar(absolute), and therefore have not been individually tested at final pressure in the full package. A small number of cooling fittings (4) and one capillary tube failed during the integration process. These were repaired in place and subsequently tested successfully.

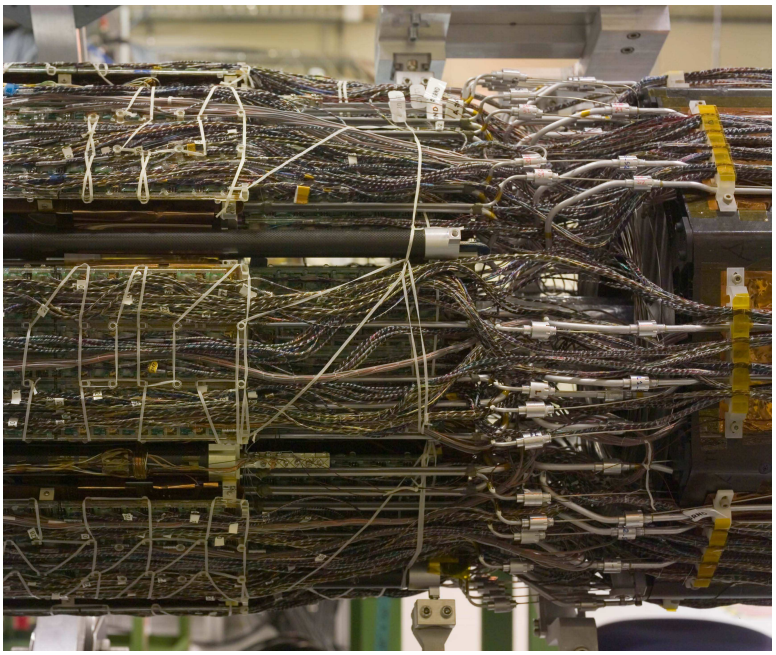

Figure 47. View of the services connection at PP0 where the detector is connected to the SQP's.

The integration of each single service panel was followed by a connectivity test. This was performed using the full readout chain and employed the same services as the endcap system test (section 8). This test checked all the electrical and optical connections, the module micro-cable mapping, the environmental sensors, the optical fiber mapping, and the functioning of the optical driver/receiver boards. Note that this test was performed without cooling. Ten micro-cables with

broken wires were found by the connectivity test. In six cases the damage was visible, clearly caused by handling, and was repaired. In three cases the damage was not visible but the modules could be recovered by using spare or redundant connections. One module was lost. No broken optical fibers were found. No significant damage to the SQPs was found.

Active component failures not caused by handling were encountered at a low level in the integrated package. One front-end readout chip failed in a disk module by developing an internal short. The module functionality except for this chip was recovered by breaking wire bonds to isolate the failed chip. Two optical components failed: one channel of a laser diode array and one channel of a photodiode array. In both cases the failure was confirmed to be internal to the component and could not be repaired. However, in both cases the affected modules were moved to spare service slots. One module was discovered with an unusual defect that prevented it from operating with the final optical communication, yet it operated with a pure electrical readout as used for production testing.

	Fractional loss (%)			
	Pixel From assembly	Fe or Module Before integration	Fe or Module After integration	Total After integration
L2	0.29	0	0	0.29
L1	0.20	0	0.20	0.40
L0	0.07	0	0	0.07
		Barrel Total		**0.28**
D1C	0.12	0	0	0.12
D2C	0.11	0	2.08	2.19
D3C	0.18	0	0.13	0.31
		Endcap C Total		**0.87**
D1A	0.14	0	0	0.14
D2A	0.10	0.13	0.13	0.23
D3A	0.26	0.13	0.13	0.39
		Endcap A Total		**0.25**
		Pixel Total		**0.33**

Table 13. Inefficiency in % for barrel and disk layers after final integration and connectivity test described in the text. Pixel inefficiencies are those seen in individual module testing (section 6) and are assumed to be the same after final integration as before. The column FE or Module indicates the fraction resulting from inoperative front-end chips or complete modules.

The data from the connectivity test, combined with the detailed production data, show that 99.7% of the detector was operational after integration (0.1% due to module/optoboard-level failures discussed above, 0.2% due to pixel-level failures already present in the staves and sectors). Table 7.6.1 summarizes the fraction of non-working parts of the pixel detector as a function of the barrel and end-cap layers prior to installation into the ATLAS Inner Detector.

Table 7.6.1 Inefficiency in % for barrel and disk layers after final integration and connectivity test described in the text. Pixel inefficiencies are those seen in individual module testing (section

6) and are assumed to be the same after final integration as before. The column FE or Module indicates the fraction resulting from inoperative front-end chips or complete modules.

8. Installation

Upon completion of the integration of the pixel detector (described in the previous section), the pixel package was transferred from the ITT to a temporary support structure, Dummy Support Tube or DST, for transport from the surface assembly building to the ATLAS detector underground.

The DST was designed to receive the detector from the integration tool in the surface assembly building and to keep it dry and protected during the transport to the ATLAS pit. The detector support conditions changed during the extraction from ITT to DST. The load was transferred from the supports on beam pipe plane, used during the integration period, to the sliders mounted on the diagonals of the lower two quadrants. A set of V-Flat rails in the DST, replicating the ones in the Pixel Support Tube, provided the new interface to the sliders by which the detector was guided first into the DST and later on, in the pit, into its final location.

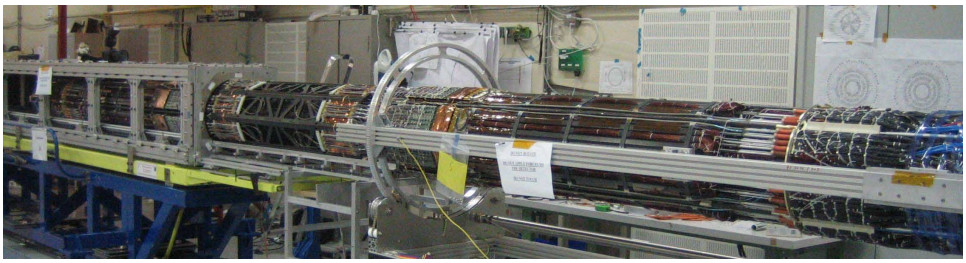

Figure 48. The pixel detector leaves the tool on which has been integrated(ITT on the right) and it enters into the transportation tool (DST on the left). The blue structure underneath the DST is equipped with pivoting and spring loaded wheels for an easy and shock free transfer outside the building.

The driving force required to move the detector was provided by a winch attached to the far end of the DST that pulled the detector by a metal line attached underneath the detector at the PP0 area.

The detector transfer to the ITT provided important information that was useful for the installation in the ATLAS underground hall. In particular:

- The very limited clearances between the detector and the Pixel Support Tube (section 7.1) were checked. In some cases, structures of the detector had to be modified to eliminate envelope violations in the PP0 area.

- The impact of the alignment on the clearance at the entrance of the PST was understood and the installation procedures updated accordingly.

- The force required to make the detector slide partially passes to the detector and validation of the estimated friction coefficient was important.

The pixel detector inside the DST was transferred from the surface assembly building to a staging area above an access shaft to the ATLAS underground cavern. A combination of a custom-wheeled cart (see the blue structure in Figure **??** and a portable crane were used. Once in the staging area, the DST was picked up by an overhead crane and slowly lowered into the ATLAS underground hall (Figure **??**a), coming to rest on a platform at the end of the ATLAS ID volume, with the ATLAS endcap-calorimeters retracted to provide sufficient room (Figure **??**b)

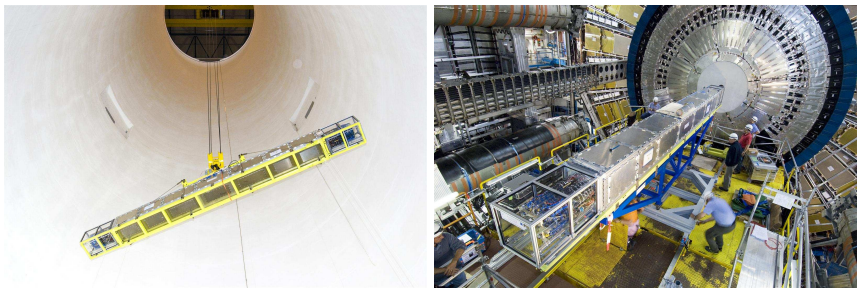

Figure 49. (a) the pixel detector in the Dummy Support Tube (see text) being lowered into the ATLAS underground hall and (b) the Dummy Support Tube and pixel detector on a platform between the Inner Detector area and the endcap calorimeter.

The DST was rotated and carefully aligned with the PST, already installed within the Inner Detector. The pixel package was slowly pulled into the PST over about a two day period. The clearance between the pixel package and the PST was very small (by design) in a number of positions along the package, requiring very careful monitoring and small last-minute adjustments. This process is illustrated in Figures **??**a and **??**b.

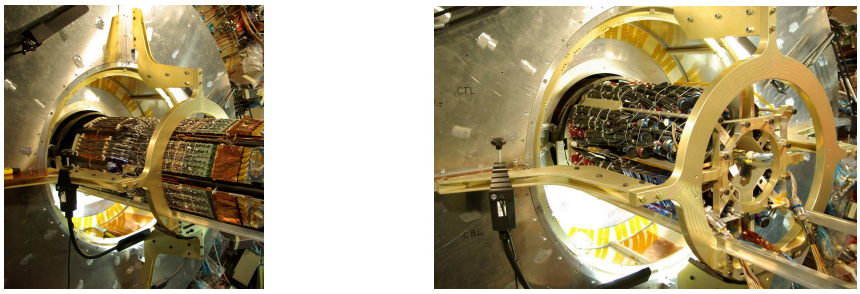

Figure 50. (a) the pixel package during transfer from the DST to the PST showing the region at the end of the inner detector and (b) just before completion of the insertion showing the temporary support of internal services at the end of the package.

The mounts attached to the pixel detector global support frame engaged the mating mounts within the PST with excellent alignment (viewed by small TV cameras). The basic installation process of the pixel package was completed by July 1, 2007.

References

[1] M. Olcese, C. Caso, G. Castiglioni, R. Cereseto, S. Cuneo, M. Dameri, C. Gemme, K. W. Glitza, G. Lenzen, and F. Mora. Ultra-light and stable composite structure to support and cool the atlas pixel detector barrel electronics modules. *Nucl. Instr. and Meth. A*, 518(3):728–737, 2004.

[2] Karl-Heinz Becks, Peter Gerlach, Karl-Walter Glitza, Pascal Knebel, Peter Mattig, Bernd Sanny, Sebastian Reuschel, Swetlana Springer, and Bernd Witt. Local support assembly of the atlas pixel detector. *Nucl. Instr. and Meth. A*, 565(1):102–105, 2006.

[3] A. Andreazza, V. Kostyukhin, and Madaras. R. Survey of the atlas pixel detector components. ATL-IP-QC-0035, CERN, Sept. 2006.

[4] E. Andersen, K. Einsweiler, D. Giugni, C. Glitza, G. Lenzen, N. Hartman, M. Garcia-Sciveres, M. Gilchriese, M. Olcese, L. Rossi, B. Sanny, E. Vigeolas, and S. Coelli. Atlas pixel detector assembly and testing of the pixel detector system. ATL-IP-QA-0007, CERN, October 2007.

[5] The panels were manufactured by Allcomp, Inc, City of Industry, California, USA).

[6] The carbon foam was also produced by Allcomp, Inc starting with reticulated vitreous carbon foam(nominal density about 0.05 g/cc). The density was increased by chemical vapor deposition at high temperature to increase the strength.

[7] Work hardening of the aluminum 1060 tubes was required to increase the resistance to internal pressure in the case of fault conditions in the cooling system. Work hardening was done by alternating internal and external pressure on each tube for about 20 cycles.

[8] The conformal coating was Parylene.

[9] The adhesive used was CGL-7018 manufactured by xxx.

[10] A. Andreazza, V. Kostyukhin and R. Madaras, *Survey of the ATLAS Pixel Detector Components*, ATL-IP-QC-0035 (2007).

[11] ATLAS Pixel Collaboration, *ATLAS Pixel Module Electrical Test Description*, ATL-IP-QP-0144 (2004).

[12] ATLAS Pixel Collaboration, *Pixel Module Test Setup Specifications*, ATL-IP-ES-0088 (2003).

[13] ATLAS Pixel Collab., *http://pixdata.lbl.gov/surf/ambush/doc/surf-html/index.html*